POLITECNICO DI TORINO
Repository ISTITUZIONALE

Mathematical model of the chronic stage of SLE including the complement protein C1q

Original
Mathematical model of the chronic stage of SLE including the complement protein C1q / Suvandjieva, V., Acotto, F., Tsacheva, I., Rashkov, P.. - In: MATHEMATICAL BIOSCIENCES. - ISSN 0025-5564. - ELETTRONICO. - 402:(2026), pp. 1-21. [10.1016/j.mbs.2026.109832]

Availability:
This version is available at: 11583/3017129 since: 2026-11-04T09:24:41Z

Publisher:
Elsevier

Published
DOI:10.1016/j.mbs.2026.109832

Terms of use:

This article is made available under terms and conditions as specified in the corresponding bibliographic description in the repository

Publisher copyright

(Article begins on next page)

28 November 2026

Mathematical Biosciences 402 (2026) 109832

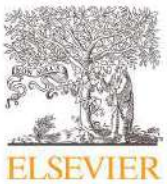

Contents lists available at ScienceDirect

Mathematical Biosciences

journal homepage: www.elsevier.com/locate/mbs

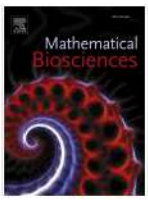

Original research article

Mathematical model of the chronic stage of SLE including the complement protein C1q

Vladimira Suvandjieva [a], Francesca Acotto [b], Ivanka Tsacheva [c], Peter Rashkov [a,*]

[a] Institute of Mathematics and Informatics, Bulgarian Academy of Sciences, ul. Akad. Georgi Bonchev, bl. 8, Safia, 1113, Bulgaria
[b] Dipartimento di Matematica "Giuseppe Peano", Università di Torino, via Carlo Alberto 10, Torino, 10123, Italy
[c] Faculty of Biology, Sofia University Sveti Kliment Ohridski, bul. Dragan Tsankov 8, Sofia, 1164, Bulgaria

ARTICLE INFO

Keywords:
Lupus
Complement system
Autoimmunity
Mathematical model
Bifurcation analysis

ABSTRACT

Systemic Lupus Erythematosus is a chronic autoimmune disease which exhibits complex pathogenesis and unpredictable course, making diagnosis and treatment particularly challenging. Understanding the dynamic interactions among the key components of the immune response is therefore of great importance. In this context, mathematical modeling is a powerful tool for investigating the disease progression and possibly the development of more effective therapy. We present a model for the chronic phase of SLE that incorporates interactions between T and B lymphocytes, dendritic cells in the role of antigen presenting cells, autoantigen, antibody, pro- and anti-inflammatory factors. What makes the model unique is the inclusion of the C1q complement protein and the immune complexes it forms. We examine whether and when periodic behaviour corresponding to the peaks and troughs typical of SLE (lupus flares) is observed. The results from the numerical experiments show that the presence of dendritic cells is essential for the existence of periodic dynamics. The model also suggests that that fluctuations in the C1q concentration that are characteristic for SLE patients may not be dependent on a reduced production of C1q in the organism.

1. Introduction

Systemic Lupus Erythematosus (SLE) is an autoimmune disease in which the immune system produces antibodies that, along with protecting the body from foreign agents, attack components of the body itself, causing inflammation and tissue damages. Such cross-reacting antibodies are referred to as autoantibodies. The heart, skin, lungs, liver, vascular endothelium, kidneys, and nervous system are often affected [1]. However, symptoms vary among people and may be mild to severe. Moreover, the prognosis of this disease is not easy to predict. SLE alternates symptomatic periods with periods of remission.

The precise cause of SLE remains uncertain. However, evidence suggests that impaired clearance of apoptotic material and/or abnormalities in the apoptotic process, together with a genetic predisposition, contribute to the onset and progression of the disease. Multiple SLE-associated autoantibodies, which are found in both SLE patients and lupus mouse models, recognize apoptosis-induced modifications of nuclear autoantigens [2].

A key concept in the pathogenesis of SLE is an imbalance between apoptotic cell production and disposal of apoptotic material from the organism [3]. In particular, serum of SLE patients contains chromatin originating from apoptotic cells. Under normal circumstances chromatin from the nucleus is translocated to the cell surface in microvesicles or blebs, and early apoptotic cells are cleared from the tissue without causing inflammation. In SLE patients, however, the blebs on the surface of an apoptotic cell rupture and spontaneously release chromatin in the tissue, triggering the adaptive immune response, and consequently, the activation of the complement system [4,5].

The complement system is a mechanism of the innate arm of the immune system, involving a large number of plasma and cell-surface proteins [6]. Its function is to complement the ability of antibodies and phagocytic cells to clear pathogens, promote inflammation, and directly destroy foreign cell membranes. There are three pathways to activate complement, one of which, the classical pathway is triggered by antibody or by direct binding of complement component C1q to the pathogen surface. The disruption and dysregulation of the complement

* Corresponding author.
E-mail addresses: vladimira.suvandjieva@math.bas.bg (V. Suvandjieva), francesca.acotto@unito.it (F. Acotto), itsacheva@biofac.uni-sofia.bg (I. Tsacheva), p.rashkov@math.bas.bg (P. Rashkov).

https://doi.org/10.1016/j.mbs.2026.109832

Available online 24 October 2026
0025-5564/© 2026 The Author(s). Published by Elsevier Inc. This is an open access article under the CC BY license (http://creativecommons.org/licenses/by/4.0/).

system in SLE is well-known [4,7]. Complement protein C1q is important for an effective clearance of apoptotic material as demonstrated by experimental mouse models. Also, C1q-deficient mice are characterised by significantly greater numbers of apoptotic bodies and autoantibody production compared with control [8].

As C1q binds to exposed nuclear material from blebs, it forms a complex that is immunogenic in itself. The persistent antigen presentation to B cells leads to the production of antibodies against C1q, which is a widely accepted hallmark of lupus [1,9]. Furthermore, production of autoantibodies against nuclear material, including chromatin, formation of immune complexes, interference with intracellular functions, and the deposition of such complexes in tissue through binding to Fc receptors causes local inflammation [3,10,11]. This process takes place, in particular, in the kidneys and contributes to endothelial injury and thrombosis.

We propose a mathematical model for the chronic stage of SLE incorporating the complement protein C1q, and its interactions with lupus antibodies that elicit response in the form of inflammation and affect the dynamics of several immune cell populations. These immune cells include dendritic cells, T helper cells, T regulatory cells, autoreactive B cells that respond to antigen and chemokine stimuli that either promote or suppress inflammation.

Aspects of the complement system has been modelled using high-dimensional models of reaction networks based on ordinary differential equations [12–15], but they are not placed in the specific context of lupus. Previous models in the literature focus on several specific aspects of lupus related to therapy: improvement of therapeutic protocols based on biomarkers [16], study of organ damage in the case of Lupus nephritis [17], or effective dose range optimisation for IL-2 therapy [18]. Other models work with aggregate features of the disease without elucidating the mechanisms behind its pathophysiology [19]. On the other hand, Suvandjieva et al. [20] proposed a model exploring the contribution of NETosis to the establishment of an autoimmune response. Further, models explore the epidemiology and model the age-specific prevalence of lupus [21,22]. There are several models describing the role of autoreactive T-cells in autoimmune diseases considering their relapse-remission nature [23–27]. However, unlike the model in this work, these models only take into account a small subset of cell populations and do not include other important components of the adaptive immunity such as complement proteins, immune complexes and cytokines. The oscillatory nature of autoimmune diseases is considered also in Matsuo and Iwasa [28] but the mathematical model presented there considers only basic innate immunity interactions.

This paper is organised as follows. Section 2 contains the equations of the model of interest. An initial analytical investigation of the system is presented in Section 3. In Section 4 we present a local sensitivity analysis that showcases the importance of model parameters associated with T regulatory cells on the model dynamics. Next, in Section 5, one-dimensional bifurcations with respect to selected parameters are explored using `MatCont`, a `MATLAB` toolbox for numerical bifurcation analysis [29]. Examples are provided on basins of attraction in the event of bistability based on the `MATLAB` toolbox `bSTAB` [30], as well as simulations of the temporal dynamics under assumptions of omission of dendritic cells in the system.

2. Mathematical model

The pathology of SLE is based on multiple processes that are very complicated, and we have to focus the model just on several most important aspects. For example, we lump together the multiple signalling factors involved in the inflammation and immune cell activation in two categories, broadly defined as activating (pro-inflammatory) cytokines and deactivating (anti-inflammatory) cytokines similar to the approach to modelling colonic inflammation in inflammatory bowel disease [31]. We furthermore simplify the multi-step process of T and B cell activation [32] to a single step in order to reduce the complexity of the model.

We consider the dynamics of the densities of several subpopulations of immune cells and the concentrations of immune complexes and cytokines. These are mature myeloid dendritic cells (mDCs) D_m, mature plasmacytoid dendritic cells (pDCs) D_p, autoreactive $CD4^+$ T helper cells T, regulatory T cells (Tregs) T_{reg}, and autoreactive B cells B. In addition, our model includes the complement protein C1q Q which plays an important role in the pathology of SLE [4,8] as well as autoantigen-containing debris resulting from necrosis or aberrant apoptosis a that is a hallmark of SLE [1,3]. Furthermore, we consider autoantibodies A, immune complexes between autoantibodies and C1q c_1, immune complexes between necrotic debris and C1q c_2, activating (pro-inflammatory) cytokines Y_1, and deactivating (anti-inflammatory) cytokines Y_2.

The model consists of 12 ODEs (1)–(12) that describe the dynamics of the system:

$$D_m' = \alpha_m D_m\left(1-\frac{D_m}{K_m}\right) - \frac{\nu_{D|reg}T_{reg}}{k_{D|reg}+T_{reg}}D_m + \upsilon_m\left(\frac{\gamma_0 a}{k_D+a}+\frac{\gamma_1 c_1}{k_D+c_1} + \frac{\gamma_2 c_2}{k_D+c_2}\right)D_m\,, \tag{1}$$

$$D_p' = \alpha_p D_p\left(1-\frac{D_p}{K_p}\right) - \frac{\nu_{D|reg}T_{reg}}{k_{D|reg}+T_{reg}}D_p + \upsilon_p\left(\frac{\gamma_1 c_1}{k_D+c_1}+\frac{\gamma_2 c_2}{k_D+c_2}\right)D_p\,, \tag{2}$$

$$T' = \left(\frac{\pi_{T|Dm}D_m}{k_{T|Dm}+D_m}+\frac{\beta_1 Y_1}{k_T+Y_1+Y_2}\right)T - \beta_T T^2 - \frac{\beta_{reg}T_{reg}}{k_{reg}+T_{reg}}T - \frac{\beta_2 Y_2}{k_T+Y_1+Y_2}T\,, \tag{3}$$

$$T_{reg}' = \sigma_{reg} + \frac{\beta_2 Y_2}{k_T+Y_1+Y_2}T + \pi_{Dm|reg}D_m T_{reg} - \mu_{reg}T_{reg}\,, \tag{4}$$

$$B' = B\left(\sigma_B + \pi_{T|B}T + \frac{\pi_{Dm|B}D_m}{k_{Dm|B}+D_m}\right) - \mu_B B^2\,, \tag{5}$$

$$a' = \frac{\sigma_a Y_1 + \sigma_A A}{1+\mu_\phi Q} - \upsilon_{[aQ]}Qa - \frac{\gamma_0 a}{k_D+a}D_m - \varepsilon_a a\,, \tag{6}$$

$$A' = \alpha_{B|A}B - \upsilon_{[AQ]}QA - \delta_A A\,, \tag{7}$$

$$Q' = \sigma_Q - (\upsilon_{[AQ]}A + \upsilon_{[aQ]}a)Q - \delta_Q Q\,, \tag{8}$$

$$c_1' = \upsilon_{[AQ]}QA - \frac{\gamma_1 c_1}{k_D+c_1}(D_m+D_p) - \Phi_1(c_1,c_2)c_1\,, \tag{9}$$

$$c_2' = \upsilon_{[aQ]}Qa - \frac{\gamma_2 c_2}{k_D+c_2}(D_m+D_p) - \Phi_2(c_1,c_2)c_2\,, \tag{10}$$

$$Y_1' = \frac{\nu_1 Y_1 + \nu_2(A+c_1+c_2)}{k_1+Y_1+Y_2} + \lambda_0 D_m + \frac{\lambda_1}{1+k_Q Q}D_p - \delta_1 Y_1\,, \tag{11}$$

$$Y_2' = \lambda_2 D_m + \lambda_3 T_{reg} - \delta_2 Y_2\,. \tag{12}$$

We introduce the equations (1)-(5) that govern the dynamics of several types of immune cell populations.

Myeloid dendritic cells. An important characteristic of mDCs D_m is that they continuously sample the tissue environment for antigen, which they process and present to T lymphocytes [33]. In SLE we note their ability to take up apoptotic and necrotic debris a or immune complexes c_1, c_2 via a Michaelis-Menten functional response with maximum rates $\gamma_i, i = 0, 1, 2$ and Michaelis constant k_D and present it to T cells in an immunogenic context. We assume in (1) the same Michaelis constant k_D for processing the antigen for the sake of simplicity. In (1) we assume that mDCs are maintained via a logistic growth law with maximal growth rate α_m and carrying capacity K_m, supplemented by activation at rate $\upsilon_m \geq 1$ from picking-up of antigen (in this case debris a or immune complexes c_1, c_2). Activated mDCs present the autoantigen to T-cells. Regulatory T cells have a deactivating effect on mDCs [34] which is modelled by a negative Michaelis-Menten term with maximum rate $\nu_{T|Dm}$ and Michaelis constant $k_{D|reg}$.

Plasmacytoid dendritic cells. Denoted by D_p these cells are the second main type of dendritic cells, which tend to accumulate in inflammatory

sites such as skin lesions in lupus, and moreover, are potent producers of pro-inflammatory signals such as IFNα [35]. Like mDCs, pDCs are assumed to follow a logistic growth law with maximal growth rate α_p and carrying capacity K_p. Regulatory T cells suppress pDC activity, a process modelled with the same Michaelis-Menten term as used in (1). In contrast to mDCs, pDCs are unable to ingest uncomplexed apoptotic debris. However, when necrotic or apoptotic debris or autoantibodies are in complex with complement protein C1q, pDCs are able to ingest these complexes [2]. We assume this antigen processing occurs with the same Michaelis-Menten functional response as for the mDCs. However, we use an activation rate $\upsilon_p \geq \upsilon_m$ in order to model the elevated potency of pDCs to become activated after exposure to antigen in the last term of equation (2). Observe that Gao et al. [18] make a similar assumption of the suppressive effect of Tregs on APCs but use a different functional response.

Autoreactive T helper cells. These CD4+ T cells T recognise peptides presented by major histocompatibility complex class II molecules and promote the function of autoreactive B cells to produce autoantibodies [33]. The dynamics of autoreactive T helper cells follows a logistic growth law (3) with carrying capacity dependent on the activating factors Michaelis-Menten functions are used for T helper cell activation pathways that involve mDCs and chemokines. First, antigen-presenting mDCs present autoantigen to autoreactive T-helper cells and activate them at maximum rate $\pi_{T|Dm}$ and Michaelis constant $k_{T|Dm}$. Second, pro-inflammatory signals (such as TNF-α, IL-6, IL-21) from the activating cytokine group (Y_1) stimulate their proliferation [36] at maximum rate β_1 and Michaelis constant k_T. Anti-inflammatory cytokines Y_2 suppress the activation and are included in the denominator. Both types of activation are represented by the first term of equation (3).

On the other hand, to prevent an uncontrolled immune response, we consider a crowding effect on T helper cells described by the term $-\beta_T T^2$, and assume a T regulatory cell-mediated suppression at maximum rate β_{reg} and Michaelis constant k_{reg} which is represented by the third term of (3). Anti-inflammatory deactivating cytokines (such as IL-2 or TGF-β) induce phenotype switching of naive T helper cells to T regulatory cells under the expression of the transcription factor Foxp3 [37] – this process occurs at maximum rate β_2 and is represented by the last term of (3).

Regulatory T cells. Naturally occurring $CD4^+CD25^+$ regulatory T cells T_{reg} [32] are assumed to have constant supply σ_{reg} – first term of (4). There is conflicting evidence whether counts of such cells in SLE patients differ from those in healthy subjects [38], so we take the reference value for σ_{reg} from healthy subjects. The second term of (4) represents phenotype switching of T cells. Under the action of anti-inflammatory cytokines (in presence of IL-2 and TGF-β) naive T helper cells switch phenotype to regulatory T cells [37]. The third term of equation (4) represents an activation by APCs. When DCs present self antigens in a tolerogenic way, regulatory T cells can be activated at rate $\pi_{Dm|reg}$ [2]. The last term of (4) represents removal of Tregs with rate μ_{reg}.

Autoreactive B cells. Dysregulated B cell responses are related to SLE onset, due to loss of tolerance at different checkpoints [1], but in order to simplify our analysis, we model all involved B lymphocytes as a single population of autoreactive B cells B. These lymphocytes are activated due to antigen-presentation by mDCs, through induction by IL-21 signals from CD4+ T cells [39], or by self-renewal at rate σ_B from memory B cells, and are capable of secreting autoantibody (7).

Activated T cells are crucial for the activation of autoreactive B cells by presenting the self epitopes from modified nuclear material and apoptotic debris, with subsequent production of antibodies directed towards modified self [2]. The dynamics of autoreactive B cells follows a logistic growth law (5) with carrying capacity dependent on the activating factors and crowding parameter μ_B. The parameter σ_B can be chosen positive in (5) if we suppose that autoreactive memory B cells have been formed, and otherwise it is set to 0. The T-cell mediated activation process occurs at rate $\pi_{T|B}$ in (5). The activation of B-cells due to contact with mDC and autoantigen presentation is assumed to follow a Michaelis-Menten functional response with maximum rate $\pi_{Dm|B}$ and Michaelis constant $k_{Dm|B}$.

A cartoon of the interactions between cell populations is shown in Fig. 1. In the model we also consider a scenario where the role of DCs is negligible, and their compartments, individually, or both are assumed equal to zero.

Next we describe the interactions between antigens, immune complexes, C1q protein of the complement system and chemokines which we divide into two generic groups: pro- and anti-inflammatory, similar to the approach of Wendelsdorf et al. [31], in order to keep model complexity to a minimum.

Autoantigen-containing debris. Autoantigen-containing apoptotic debris a that might be capable of breaking immune tolerance originates from apoptotic blebs (containing modified DNA and RNA residues) is assumed to be produced as a result of TNF-induced cell death or tissue damage [40]. Its formation depends on the level of pro-inflammatory cytokines $\sigma_a Y_1$, and on the level of circulating autoantibody $\sigma_A A$ which damages cells in tissues or forms complexes with nuclear and non-nuclear material in the extracellular space [41]. C1q clears the apoptotic debris by direct binding and facilitates its phagocytosis by macrophages [42]. Hence, we include in the denominator of the formation term a factor $(1 + \mu_\phi Q)$ in order to capture that high levels of C1q prevent the formation of apoptotic debris (larger values of μ_ϕ represent a stronger suppression of apoptotic debris formation by C1q binding in the first term in the right-hand side of Eq. (6)). Conversely, under C1q deficiency the level of apoptotic residue in the circulation increases triggering an increased formation of necrotic material and apoptotic debris a [43].

We assume two pathways of removal of apoptotic debris in (6). First, it is cleared by the complement system (binding to C1q) at rate $\upsilon_{[aQ]}$. Second, mDCs which play the role of antigen presenting cells (APCs) ingest it, with limited pick-up capacity - a Michaelis-Menten function $\frac{\gamma_0 a}{k_D + a}$ is chosen to represent this process. Removal by other means is assumed to be slow and is represented by the final term $-\varepsilon_a a$:

Autoantibody. Following activation, the autoreactive B cells mature, expand, and produce antibody at rate $\alpha_{B|A}$, amplifying the adaptive

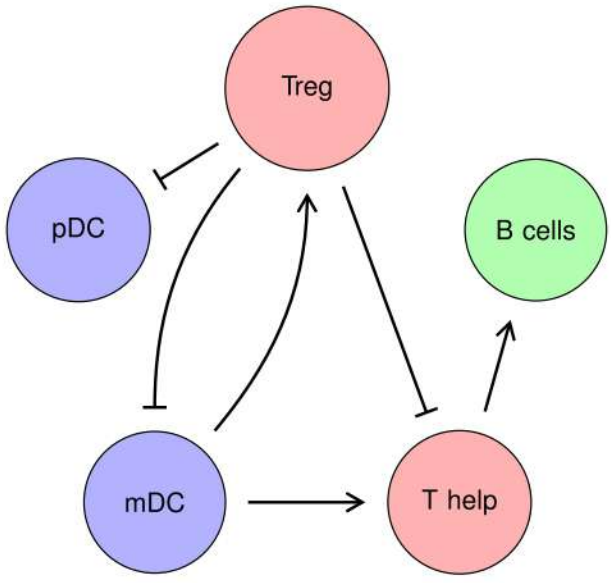

Fig. 1. Interactions between the immune cell populations. Sharp arrows (→) indicate activation, while blunt arrows (⊣) – deactivation.

immune response [3,39]. Autoantibodies and the complement protein C1q form complexes [4] – a second-order process represented by the second term of (7), occurring at rate $\upsilon_{[AQ]}$. The last term of (7) stands for the natural decay of autoantibodies with rate δ_A.

Complement protein C1q. The complement protein C1q is produced by tissue-resident macrophages and in the liver at constant rate $\sigma_Q > 0$ [44]. It is the molecule that initiates the classical pathway of the complement system [45]. We model the formation of immune complexes between C1q and autoantibody, and between C1q and necrotic residue as second-order processes at rates $\upsilon_{[AQ]}$ and $\upsilon_{[aQ]}$ respectively in (8). Removal of C1q occurs at rate δ_Q and is modelled in the last term of (8). We consider a simplified framework with constant supply of C1q because of insufficient data on complement activating molecules present on the surface of apoptotic cells [4].

Immune complexes between autoantibody and C1q. The formation of immune complexes between C1q Q and autoantibody A is modelled as a second-order reaction with rate $\upsilon_{[AQ]}$ in (9).

Under homeostatic conditions immune complexes bind to erythrocytes and are picked up by mononuclear phagocyte system in the liver or spleen via an engagement of the antibody Fc domains to the Fc receptors of the phagocytes. As the Fc receptor function is impaired in SLE, this fact may predispose the organism to deposit the circulating immune complexes in the kidney instead [46]. Hence we choose to model the clearance Φ_1 through the kidneys with a density-dependent clearance rate

$$\Phi_1(c_1, c_2) = \frac{\mu_1}{1 + \rho(c_1 + c_2)} + \varepsilon$$

where the constants μ_1 and $\varepsilon \approx 0$ indicate the upper and lower asymptotes of Φ_1. The saturation constant ρ takes into account the competitive effect between the two types of immune complexes involving C1q c_1, c_2. This immune complex is also ingested by mDCs and pDCs, a process modelled by Michaelis-Menten term with maximum rate γ_1 (second term of Eq. (9)).

The kidney is an important organ in SLE because it is involved in more than 50% of the SLE patients (*Lupus nephritis*) and is a major morbidity factor [1].

Immune complexes between C1q and apoptotic debris. The formation of immune complex between C1q Q and apoptotic debris a is modelled as a second-order reaction with rate $\upsilon_{[aQ]}$ [4]. It is cleared through the kidneys again at density-dependent clearance rate

$$\Phi_2(c_1, c_2) = \frac{\mu_2}{1 + \rho(c_1 + c_2)} + \varepsilon$$

where the constants μ_2 and $\varepsilon \approx 0$ indicate the upper and lower asymptotes. Similarly to (9), the saturation constant ρ takes into account the competitive effect between the two types of immune complexes involving C1q c_1, c_2. c_2 is ingested by mDCs and pDCs, which is modelled with Michaelis-Menten functional dependence with maximum rate γ_2 (second term of Eq. (10)). We do not consider autoantibody A (anti-C1q antibody) binding to autoantigen a or immune complexes between C1q and apoptotic debris c_2 because of complex conformational changes [45].

Pro-inflammatory cytokines. This group includes signalling factors like TNF-α, IFN-γ, or IL-6, involved in the SLE pathogenesis [3]. The production of pro-inflammatory cytokines Y_1 is assumed to follow several pathways in Eq. (11): first, as a result of autocrine stimulation of various cell types with maximal rate ν_1, second as a result of deposition of autoantibody and immune complexes with C1q in tissue which cause local inflammation (with maximal rate ν_2) [3,10]. Immune complexes activate complement and, through binding Fc receptors, drive inflammation [3], and in particular, C1q destroys cells with deposits of autoantibody immune complexes on their surface. This causes damage to the tissues and leads to local inflammation and increased production of Y_1. We assume this process to be self-limiting with Michaelis constant k_1.

In the denominator of the first term of Eq. (11) we include a suppressive effect of the anti-inflammatory cytokine group Y_2 that affects multiple cell phenotypes causing a reduction in the production of pro-inflammatory stimuli and counterbalances the inflammatory process similar to the approach of Baker et al. [47]. Moreover, pro-inflammatory cytokines are produced due to activity of dendritic cells. mDCs produce Y_1 at rate λ_0 and pDCs produce it at maximum rate λ_1. However, C1q suppresses IFNα production by pDCs, which we represent by the factor $1/(1 + k_Q Q)$ in the third term of Eq. (11) [45,48]. These maximum rates are assumed to satisfy $\lambda_0 \ll \lambda_1$ to account for the ability of pDCs to secrete large amounts of type-1 interferon (IFNα). The pro-inflammatory cytokines have clearance rate δ_1.

Anti-inflammatory cytokines. We consider a generic group of anti-inflammatory cytokines Y_2 like Wendelsdorf et al. [31] did in order to reduce our model's complexity. The terms in Eq. (12) represent anti-inflammatory (deactivating) cytokines such as TGF-β, IL-10 produced by mDCs at rate λ_2, and by T regulatory cells at rate $\lambda_3 < \lambda_2$ to account for the fact that these cells have deficient suppressive activity in SLE [49]. The clearance rate of Y_2 is δ_2.

The units of measurement of cell populations are cells/mL and for the soluble factors are μg/mL. However, for the sake of clarity in the presentation, in the figures containing profiles of cytokines Y_1 and Y_2 their units of measurement are pg/mL (10^{-6}μg/mL).

2.1. Parameter values

The model (1)–(12) contains a large number of parameters, some of which can be found in the literature, some – estimated, and others have assumed values, or have their values varied in order to explore the dynamical properties of the model. The parameter values are listed in Table 1. We provide derivation of several parameter values from experimental data below:

1. To estimate the value of K_p in (2), we use the estimate that pDCs are about 0.4% of peripheral blood mononuclear cells (PBMC). For healthy donors the PBMC yield ranges from 0.5×10^6 to 3×10^6 cells per mL blood [50]. This leaves a range of 200–1200 pDC/mL blood. We use thus a slightly larger value for the carrying capacity $K_p = 1300$ cells/mL in order to account for the suppressive effect of regulatory T cells in (2).
2. For the rates λ_0, λ_1 we use the data provided in [51] from which it is visible that around 200 pg/ml of INF-γ is produced for two days by dendritic cells, or around 100 pg/ml per day. Considering that the normal range of dendritic cells is around 1000 per ml blood, we estimate that the values of λ_0 and λ_1 should have order 10^{-1} pg/(cell day), or 10^{-7} μg/(cell day).
3. The value of λ_3 is chosen 1000 times smaller than λ_2 to represent the dysregulation of Tregs in SLE, and their reduced ability to produce anti-inflammatory cytokines.
4. For the parameter μ_B we use the data provided in Macallan et al. [52, Table 1] the following way: from the data on Proliferation and disappearance rates of B cells in young and elderly healthy subjects, we take the average percentage for elderly and young individuals:
$$\mu_B = \frac{3.94 + 5.21}{2} \times 0.01 = 0.046.$$
5. For the parameter μ_{reg} we take data from Macallan et al. [53, Table 1] and take the average of the disappearance rates for $CD4^+CD45RO^+$ and $CD4^+CD45RA^+$ and multiply it by 0.01 as it is given as percentage:
$$\mu_{reg} = \frac{7.37 + 7.25}{2} \times 0.01 = 0.07.$$
On the other hand from the data provided in [54] the parameter for turnover of regulatory T cell (d_{G_T} in the notation in Kim et al. [54]) is 0.1. Therefore, for μ_{reg} we take values in the interval $[0.07, 0.1]$.

6. For σ_{reg} we use the data from Macallan et al. [53, Table 1]. We take the average of $CD4^+CD45RO^+$ and $CD4^+CD45RA^+$ proliferation rates, multiply it by 0.01 as it is given as percentage and finally multiply the result by a number between 1 and 5 taking into account that the normal range of T-cells in the human body is between 1000 and 5000 cells per mL.

$$\sigma_{reg} = \frac{2.65 + 0.59}{2} \times 0.01 \times n,$$

where $n \in [1000, 5000]$ and the range for σ_{reg} is the interval $[0.0162, 0.081]$.
7. The maximum activation rate of naive $CD4^+$ T cells β_1 is taken from Lee et al. [55, Table 2: parameter π_{H1}].
8. The value for β_2 is taken from Kim et al. [54, Table 1], and represents conversion of CD4+ T cells to regulatory T cell under the influence of TGF-β.
9. As reference values for δ_1 and δ_2 we use the rates of turnover of IL-2 and TGF-β, adapted from Kim et al. [54, Table 1]. The maximum clearance rates for the two immune complexes μ_1, μ_2 are assumed to be of the same order.
10. To estimate σ_Q we use the study van Schaarenburga et al. [56]: the amount of C1q produced for 48 h is 64.6 ng/ml and 318.4 ng/ml by macrophages and dendritic cells, respectively. In total that makes 382.2 ng/ml or 0.38 μg/ml for 48 h, which is 0.19 μg/ml for 24 h.
11. To estimate the removal rate of C1q δ_Q, we use the experimental data in [57]. We obtain that the half-life of C1q is approximately 12.5 h, which gives $\delta_Q \approx \ln 2/(12.5/24) \approx 1.33$ day^{-1}.
12. The maximum clearance rates of C1q complexes with autoantibody and apoptotic debris $\mu_i, i = 1, 2$ are assumed lower than the removal rates of C1q and autoantibody because of the higher molecular volume of the complexes.

Parameter values in Table 1 that have assumed values are chosen in order to produce values of model variables within physiologically reasonable ranges.

3. Properties of the analytic solution

We state some properties of the analytic solution of the model presented in Section 2 which ensure that all unknown variables retain their biological meaning.

Theorem 1. *The solutions to the model (1)–(12) in Section 2 remain non-negative in time $t > 0$ for non-negative initial values.*

The proof of Theorem 1 is given in Appendix A.1.

Theorem 2. *Let $\pi_{Dm|reg}$ satisfy*

$$\pi_{D_m|reg} < \frac{\mu_{reg}\alpha_m}{K_m(\alpha_m + \upsilon_m(\gamma_0 + \gamma_1 + \gamma_2))}.$$

The solutions to the model (1)–(12) in Section 2 remain uniformly bounded in time $t > 0$ for non-negative initial values.

The proof of Theorem 2 is given in Appendix A.2.

Theorems 1 and 2 together imply that the solution to the model is biologically feasible for all $t > 0$ for non-negative initial conditions. In all of our numerical experiments we use values for $\pi_{D_m|reg}$ that fulfil the inequality from Theorem 2.

We have the following asymptotic dynamics

Theorem 3. *The dynamics of the model (1)–(12) in Section 2 satisfy*

$$\liminf_{t\to+\infty} T_{reg}(t) \geq \frac{\sigma_{reg}}{\mu_{reg}}, \tag{13}$$

$$\liminf_{t\to+\infty} Y_2(t) \geq \frac{\lambda_3\sigma_{reg}}{\delta_2\mu_{reg}}. \tag{14}$$

Whenever $\alpha_m + \upsilon_m(\gamma_0 + \gamma_1 + \gamma_2) < \frac{\nu_{D|reg}\sigma_{reg}}{k_{D|reg}\mu_{reg}+\sigma_{reg}}$,

$$\limsup_{t\to+\infty} D_m(t) = 0. \tag{15}$$

Whenever $\alpha_p + \upsilon_p(\gamma_1 + \gamma_2) < \frac{\nu_{D|reg}\sigma_{reg}}{k_{D|reg}\mu_{reg}+\sigma_{reg}}$,

$$\limsup_{t\to+\infty} D_p(t) = 0. \tag{16}$$

proof The estimates in (13) and (14) follow from Theorem 1, which leads from (4) to

$$T_{reg}(t)' \geq \sigma_{reg} - \mu_{reg}T_{reg}(t), \quad \forall t \geq 0,$$

and from (12) to

$$Y_2(t)' \geq \lambda_3 T_{reg}(t) - \delta_2 Y_2(t), \quad \forall t \geq 0.$$

Application of Gronwall's lemma concludes these estimates.

Let $p_m = \alpha_m + \upsilon_m(\gamma_0 + \gamma_1 + \gamma_2) - \frac{\nu_{D|reg}\sigma_{reg}}{k_{D|reg}\mu_{reg}+\sigma_{reg}}$. We have assumed $p_m < 0$. To demonstrate (15) we note from (1) that

$$\begin{aligned} D_m' &< \alpha_m D_m - \frac{\nu_{D|reg}T_{reg}}{k_{D|reg} + T_{reg}} D_m + \upsilon_m\left(\frac{\gamma_0 a}{k_D + a} + \frac{\gamma_1 c_1}{k_D + c_1} + \frac{\gamma_2 c_2}{k_D + c_2}\right) D_m \\ &< \left[\alpha_m + \upsilon_m(\gamma_0 + \gamma_1 + \gamma_2) - \frac{\nu_{D|reg}T_{reg}}{k_{D|reg} + T_{reg}}\right] D_m < D_m p_m \end{aligned} \tag{17}$$

or $D_m(t) = \mathcal{O}(e^{p_m t})$. Since $p_m < 0$, the claim of (15) follows.

The proof of (16) is analogous. *proof.* The statement of Theorem 3 reflects the observation that the density of Tregs is always greater than a positive quantity due to the naturally occurring regulatory T cells. The other statement reveals that certain parameter combinations lead to situation in which dendritic cells densities tend to zero and therefore we will analyse the cases when one or both variables D_m and D_p are equal to zero.

4. Local sensitivity analysis

In order to understand whether and how strongly model variables respond to changes in various parameters, we perform local sensitivity analysis for the variables with high biological relevance for the SLE pathology: autoantibody A, C1q protein Q, both types of immune complexes (c_1, c_2) and apoptotic debris a. This analysis allows us to understand better the relative importance of the interactions described by different parameters for these disease markers.

Sensitivity indices measure the relative change in a model variable at a certain time point $t > 0$ when a parameter changes. To compute the local sensitivity indices we select an initial state of the model and a finite mesh of time points $\{t_i > 0 : i = 1, \ldots\}$ and define the sensitivity matrix S as follows. For a parameter $\{\theta_j\}_{j=1}^m$ of the model, the ijth element of the matrix $S_{ij} = \frac{\partial z_i}{z_i}\frac{\theta_j}{\partial\theta_j}$ is the ratio of the relative change $\frac{\partial z_i}{z_i}$ in the model outcome $z_i = z(t_i)$ for the time point t_i to the relative change $\frac{\partial\theta_j}{\theta_j}$ in the parameter θ_j. The quantities S_{ij} are dimensionless and normalised, and help us understand the effect of changes of the selected m individual parameters on the model outcome [62].

In our numerical experiment we examine the phase variables $z \in \{A, Q, c_1, c_2, a\}$ and compute the trajectory on the time interval $[0, 300]$ with time step 0.1. The mesh of time points where the model output z is evaluated is $\{t_i = 250 + 0.2i : i = 0, 1, \ldots 250\}$. As measures of the normalised local sensitivity to the parameter θ_j, we use the following quantities: the extrema $s_j^{\min} = \min_i S_{ij}$ and $s_j^{\max} = \max_i S_{ij}$, the mean

$$s_j^{\text{mean}} = \frac{1}{251}\sum_{i=0}^{250} S_{ij},$$

and the ℓ^p-norms

$$\|s_j\|_p = \frac{1}{251}\left(\sum_{i=0}^{250} |S_{ij}|^p\right)^{1/p}, \quad p = 1, 2.$$

The larger the value $\|s_j\|_1$, the heavier is the influence of θ_j on the model output. If $|s_j^{\text{mean}}| \approx \|s_j\|_1$, then most elements $\{S_{ij}\}_{i=1,2\ldots}$ have the same sign, indicating a consistent effect of the change in the parameter θ_j along the trajectory $\{z_i\}$. Differences between $|s_j^{\text{mean}}|$ and $\|s_j\|_1$, as well

Table 1
Parameter definitions and values used in the numerical experiments.

Parameter	Definition	Value range	Unit	Reference
$\alpha_{B\|A}$	Production rate of autoantibodies	$(2.9, 6) \times 10^{-7}$	$\mu g/(\text{cell day})^{-1}$	[58]
α_m	Max growth rate of mDCs	10	day^{-1}	[55]
α_p	Max growth rate of pDCs	10	day^{-1}	[55]
β_1	Max activation rate of T-helper cells by pro-inflammatory cytokines Y_1	1.5	day^{-1}	[55]
β_2	Max conversion rate of T-helper cells to Tregs due to anti-inflammatory cytokines Y_2	0.022	day^{-1}	[54]
β_{reg}	Max termination rate of T helper due to contact with Tregs	0.05	day^{-1}	assumed
β_T	Crowding coefficient, T-helper	10^{-4}	$\text{cell}^{-1}\ \text{day}^{-1}$	assumed
γ_0	Max pick-up rate of apoptotic debris by DCs	0.001	$\mu g\ \text{cell}^{-1}\ \text{day}^{-1}$	Suvandjieva et al. [20]
γ_1	Max pick-up rate of complex c_1 by DCs	0.005	$\mu g\ \text{cell}^{-1}\ \text{day}^{-1}$	Suvandjieva et al. [20]
γ_2	Max pick-up rate of complex c_2 by DCs	0.005	$\mu g\ \text{cell}^{-1}\ \text{day}^{-1}$	Suvandjieva et al. [20]
δ_1	Removal rate of Y_1	12.5	day^{-1}	[54]
δ_2	Removal rate of Y_2	14.3	day^{-1}	[54]
δ_A	Autoantibody removal rate	0.73	day^{-1}	[59]
δ_Q	Removal rate of C1q	1.33	day^{-1}	[57]
λ_0	Production rate of Y_1 by mDCs and pDCs	10^{-7}	$\mu g\ \text{cell}^{-1}\ \text{day}^{-1}$	[51]
λ_1	Production rate of Y_1 by pDCs and pDCs	0.27×10^{-6}	$\mu g\ \text{cell}^{-1}\ \text{day}^{-1}$	[51]
λ_2	Production rate of Y_2 by mDCs	0.27×10^{-6}	$\mu g\ \text{cell}^{-1}\ \text{day}^{-1}$	similar to λ_1
λ_3	Production rate of Y_2 by T reg	2.7×10^{-10}	$\mu g\ \text{cell}^{-1}\ \text{day}^{-1}$	assumed $\ll \lambda_2$
μ_1	maximum clearance rate, C1q-autoAb complex		day^{-1}	assumed $\leq \min\{\delta_Q, \delta_A\}$
μ_2	maximum clearance rate, C1q-necrotic complexes		day^{-1}	assumed $\leq \delta_Q$
μ_B	Crowding coefficient, autoreactive B cells	4.6×10^{-5}	day^{-1}	[52]
μ_{reg}	Tregs death rate	(0.07, 0.1)	day^{-1}	[53,54]
μ_ϕ	Effect of C1q binding on apoptotic debris formation		day^{-1}	assumed $\leq \delta_Q$
ν_1	Max rate of autocrine production of Y_1	10^{-7}	$\mu g\ \text{ml}^{-1}\text{day}^{-1}$	assumed
ν_2	Production rate of Y_1 by deposition of immune complexes	0.5×10^{-12}	$\mu g\ \text{ml}^{-1}\text{day}^{-1}$	assumed
$\nu_{D\|reg}$	Max deactivation rate of mature mDCs/pDCs by Tregs	25 (1,120)	day^{-1}	assumed
$\pi_{T\|Dm}$	Max activation rate of T-help cells by mDCs	20	day^{-1}	assumed
$\pi_{Dm\|B}$	Max proliferation rate of B-cells due to contact with mDCs	0.1	day^{-1}	[55]
$\pi_{T\|B}$	Max proliferation rate of B-cells due to contact with T-help	0.1	day^{-1}	[55]
$\pi_{Dm\|reg}$	Activation of Tregs by mDCs		$(\text{cells/ml})^{-1}\ \text{day}^{-1}$	as indicated
ϱ	saturation constant, clearance C1q-Ab or C1q-necrotic complex	$10^3 - 10^5$	$(\mu g/\text{ml})^{-1}$	assumed
σ_a	Conversion factor of necrotic debris yield as a result of pro-inflammatory cytokines	10^4	dimensionless	assumed
σ_A	Conversion factor, Necrotic debris yield as a result of autoantibody deposits	0.01	dimensionless	assumed
σ_B	production of autoreactive B-cells	0	day^{-1}	[52]
σ_{reg}	production of Treg cells	70	cells/ml day^{-1}	[53]
σ_Q	production of C1q	0.19	$\mu g/\text{ml day}^{-1}$	[56]
k_1	Michaelis constant	0.5×10^{-6}	$\mu g/\text{ml}$	same order as k_T
k_D	Michaelis constant	0.5	$\mu g/\text{ml}$	assumed
k_Q	Michaelis constant	0.25×10^{-6}	$\mu g/\text{ml}$	same order as k_T
k_T	Michaelis constant	0.73×10^{-6}	$\mu g/\text{ml}$	[54]
$k_{Dm\|B}$	Michaelis constant	0.1	$(\text{cells/ml})^{-1}\ \text{day}^{-1}$	assumed
$k_{D\|reg}$	Michaelis constant, deactivation rate of mature mDCs/pDCs by Tregs	10^4	$(\text{cells/ml})^{-1}\ \text{day}^{-1}$	assumed
$k_{T\|Dm}$	Michaelis constant	12.5	cells/ml	[55]
k_{reg}	Michaelis constant	1	cells/ml	[55]
K_m	Carrying capacity of mDCs	13×10^3	cells/ml	[60]
K_p	Carrying capacity of pDCs	$(0.2, 1.2) \times 10^3$	cells/ml	Merck [50]
$\upsilon_{[AQ]}$	Formation rate of C1q-Ab complex $[c_1]$	0.017	$(\mu g/\text{ml})^{-1}\ \text{day}^{-1}$	[61]
$\upsilon_{[aQ]}$	Formation rate of C1q-necrotic complex $[c_2]$	0.017	$(\mu g/\text{ml})^{-1}\ \text{day}^{-1}$	[61]
υ_m	activation rate of mDCs by immune complex and antigens	1	cells/μg	assumed
υ_p	activation rate of pDCs by immune complex	{1; 10}	cells/μg	assumed

as between $s_j^{\min}$ and $s_j^{\max}$ are a sign of temporal variability in the output z over the interval in consideration. When $s_j^{\text{mean}} \approx \|s_j\|_1$, changes in the output z are positively correlated to parameter variations in θ_j. Similarly, If $s_j^{\text{mean}} \approx -\|s_j\|_1$, changes in the variable z are negatively correlated to parameter variations in θ_j. If we rank those parameters θ_j according to the magnitude of local normalised sensitivity index s_j^{mean}, we obtain a ranking of the importance of the changes of individual parameters on the outputs of interest.

The local sensitivity analysis is performed numerically in R with the help of the FME toolbox [63]. The parameter values are indicated in Table 1. The initial values are given in (18) and represent a situation where we evaluate the local sensitivity index at a low-inflammation, low disease activity state:

$$D_m(0) = 0.01; D_p(0) = 0.01; T(0) = 15; T_{reg}(0) = 700; B(0) = 60; a(0) = 10^{-5}; A(0) = 0.01; Q(0) = 0.35; c_1(0) = c_2(0) = 0; Y_1(0) = Y_2(0) = 10^{-7}. \quad (18)$$

In (18), we have low concentration of apoptotic debris in the organism, low counts of activated DCs, low counts of T and B cells, low amount of autoantibody and pro- and anti-inflammatory cytokines, and absent immune complexes, but homeostatic level of Tregs and C1q [44,53,56].

The results for the normalised local sensitivity indices s_j^{mean} of the model parameters are shown in Figs. 2 and 3 (in the case of Q, full values for the normalised sensitivity index of the C1q production rate σ_Q are provided in Table A in the Supplementary Material because they are much higher than the others). The numerical values for the sensitivities of A, a, c_1, c_2 are given in Tables B-E in the Supplementary Material. We observe that parameters with the highest local sensitivity indices for A and Q relate to the action of T regulatory cells on DCs $\nu_{D|reg}$, the Tregs removal rate μ_{reg}, and their activation by anti-inflammatory cytokines β_2, as well as the production rates of anti-inflammatory cytokines λ_2, λ_2 (Fig. 2). Not unexpectedly, the rate of production of C1q σ_Q, has the highest sensitivity index for Q. Similar behaviour is observed for the apoptotic debris variable a (Fig. 3), except that here the production rates of pro-inflammatory cytokines λ_0, λ_1 have a major effect). For the last two variables c_1 and c_2 we observe that in addition to the already listed parameters for A, Q and a, the maximal clearance rates of the immune complexes (μ_1 and μ_2) also have high local sensitivity indices (Fig. 3).

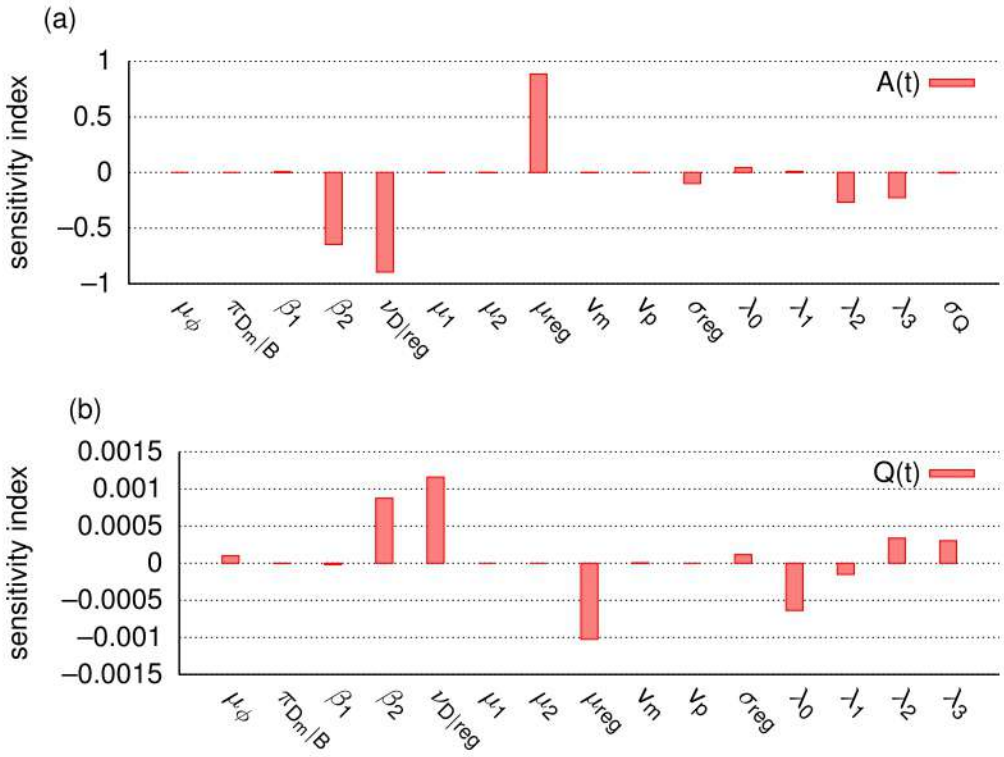

Fig. 2. Normalised local sensitivity indices for the variables A (a) and Q (b).

Moreover, other parameters with not negligible local sensitivity indices are the following: the effect of C1q binding on apoptotic debris formation, μ_ϕ, for Q, a, and c_2; the production of Treg cells, σ_{reg}, for all five variables considered. In particular, the most sensitive parameters, considering the absolute values of the sensitivity indices, are as follows:

- A: $\nu_{D|reg}$, μ_{reg}, β_2, σ_{reg}, λ_2, λ_3;
- Q: σ_Q, $\nu_{D|reg}$, β_2, μ_{reg}, σ_{reg}, μ_ϕ, λ_0, λ_2, λ_1, λ_3;
- a: σ_Q, λ_0, λ_1, β_2, μ_{reg}, $\nu_{D|reg}$, μ_ϕ;
- c_1: σ_Q, μ_1, β_2, $\nu_{D|reg}$, μ_{reg}, λ_2, λ_3, μ_2, λ_0, σ_{reg};
- c_2: σ_Q, μ_2, β_2, μ_1, μ_{reg}, μ_ϕ, σ_{reg}, λ_0, λ_1.

5. Bifurcation analysis

5.1. Equilibria

The model (1)–(12) is highly nonlinear. Thus, finding analytical expressions for the coordinates of the equilibrium points

$$(\hat{D}_m, \hat{D}_p, \hat{T}, \hat{T}_{reg}, \hat{B}, \hat{a}, \hat{A}, \hat{Q}, \hat{c}_1, \hat{c}_2, \hat{Y}_1, \hat{Y}_2)$$

is difficult due to the strong non-linear coupling of the right-hand side of the model equations.

Hence, we focus our attention on some classes of potential equilibrium points which lie on the boundary of the biologically relevant domain $\mathbb{R}^{12}_+$, and we order them by some coordinates that are 0, and others are strictly positive.

1. Equilibrium E_1 with $\hat{T}_{reg} = \frac{\sigma_{reg}}{\mu_{reg}}, \hat{Y}_2 = \frac{\lambda_3\sigma_{reg}}{\delta_2\mu_{reg}}, \hat{Q} = \frac{\sigma_Q}{\delta_Q} > 0$, the remaining phase variables equal to 0. This point corresponds to homeostasis, where no autoreactive T or B cells are present. One of the roots of the characteristic polynomial of the Jacobian matrix $f(\Lambda)$ is $\Lambda_0 = \sigma_B$ which is either zero, or positive, depending on the choice of σ_B. In the case $\sigma_B > 0$ we can conclude that this equilibrium is unstable. However, when $\sigma_B = 0$, which is the case we consider in the numerical experiments, it is impossible to make a conclusion about the stability of the equilibrium due to the complexity of the other roots of the characteristic polynomial $f(\Lambda)$.
2. Equilibria with $\hat{D}_m = \hat{D}_p = 0$ (no activated dendritic cells). There are three types of equilibrium points for which we may state the following:
   (a) equilibrium E_{2a} with $\hat{B} = \hat{A} = \hat{c}_1 = 0$, while $\hat{a} = a^*, \hat{T} = T^*, \hat{T}_{reg} = T^*_{reg}, \hat{c}_2 = c^*_2, \hat{Q} = Q^*, \hat{Y}_1 = Y^*_1, \hat{Y}_2 = Y^*_2 > 0$. One of the roots of the characteristic polynomial of the Jacobian matrix $f(\Lambda)$ is $\Lambda_1 = \sigma_B + \pi_{T|B}T^* > 0$ and therefore this equilibrium (whenever it exists) is unstable. Thus, an equilibrium with positive quantity of autoreactive T cells and no autoreactive B cells, which exists, is unstable.
   (b) equilibrium E_{2b} with $\hat{T} = 0$ (no autoreactive T cells), while $\hat{T}_{reg} = T^*_{reg}, \hat{B} = B^*, \hat{A} = A^*, a = a^*, \hat{c}_1 = c^*_1, \hat{c}_2 = c^*_2, \hat{Q} = Q^*, \hat{Y}_1 = Y^*_1, \hat{Y}_2 = Y^*_2 > 0$. One of the roots of the characteristic polynomial of the Jacobian matrix evaluated at E_{2b}, $f(\Lambda)$ is

$$\Lambda_1 = \alpha_p + \upsilon_p\left(\frac{c^*_1}{k_D + c^*_1}\gamma_1 + \frac{c^*_2}{k_D + c^*_2}\gamma_2\right) - \frac{\nu_{D|reg}\hat{T}_{reg}}{k_{D|reg} + \hat{T}_{reg}} > \alpha_p - \nu_{D|reg}. \tag{19}$$

   If the parameters satisfy $\alpha_p > \nu_{D|reg}$, the eigenvalue $\Lambda_1 > 0$ and the equilibrium E_{2b} (whenever it exists) becomes unstable. Note that the converse statement may not necessarily hold as we cannot say anything about the other roots of $f(\Lambda)$.
   (c) equilibrium E_{2c} with $\hat{T} = T^*, \hat{T}_{reg} = T^*_{reg}, \hat{B} = B^*, \hat{A} = A^*, \hat{a} = a^*, \hat{c}_1 = c^*_1, \hat{c}_2 = c^*_2, \hat{Q} = Q^*, \hat{Y}_1 = Y^*_1, \hat{Y}_2 = Y^*_2 > 0$. One root of the characteristic polynomial $f(\Lambda)$ is given by a similar expression as (19). If we take $\alpha_p > \nu_{D|reg}$, the eigenvalue is positive so the equilibrium E_{2c} (whenever it exists) is unstable.
3. Let $\hat{D}_m = 0, \hat{D}_p = D^*_p > 0$. There are two types of equilibrium points for which we may state the following:

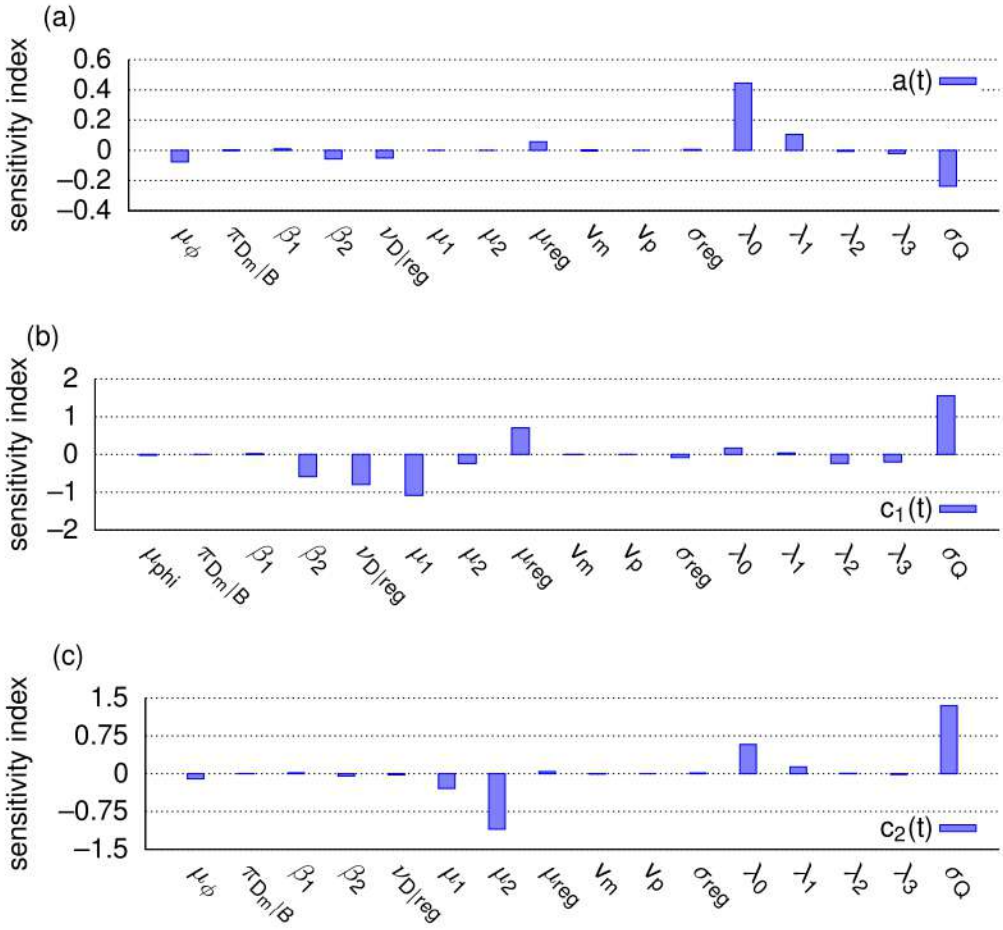

Fig. 3. Normalised local sensitivity indices for the variables a (a), c_1 (b) and c_2 (c).

(a) equilibrium E_{3a} with $\hat{B} = \hat{A} = \hat{c}_1 = 0$, whereas $\hat{a} = a^*, \hat{T} = T^*, \hat{T}_{reg} = T^*_{reg}, \hat{c}_2 = c^*_2, \hat{Q} = Q^*, \hat{Y}_1 = Y^*_1, \hat{Y}_2 = Y^*_2 > 0$.

One root of the characteristic polynomial of the Jacobian at E_{3a} is $\Lambda_1 = \sigma_B + \pi_{T|B} T^* > 0$ and therefore this equilibrium (whenever it exists) is always unstable.

(b) equilibrium E_{3b} with $\hat{T} = T^* \geq 0$ and $\hat{a} = a^*, \hat{T}_{reg} = T^*_{reg}, \hat{B} = B^*, \hat{A} = A^*, \hat{c}_1 = c^*_1, \hat{c}_2 = c^*_2, \hat{Q} = Q^*, \hat{Y}_1 = Y^*_1, \hat{Y}_2 = Y^*_2 > 0$.

The characteristic polynomial of the Jacobian at E_{3b} has a root $\Lambda_1 = \alpha_m + \upsilon_m\left(\frac{c^*_1}{k_D + c^*_1}\gamma_1 + \frac{c^*_2}{k_D + c^*_2}\gamma_2 + \frac{\gamma_0 a^*}{k_D + a^*}\right) - \frac{\nu_{D|reg}\hat{T}_{reg}}{k_{D|reg} + \hat{T}_{reg}} > \alpha_m - \nu_{D|reg}$. If we take $\alpha_m > \nu_{D|reg}$, the eigenvalue $\Lambda_1 > 0$, so this equilibrium (in case it exists) is unstable.

4. Let $\hat{D}_p = 0, \hat{D}_m = D^*_m > 0$. There are two types of equilibrium points for which we may state the following:

(a) equilibrium E_{4a} with $\hat{B} = \hat{A} = \hat{c}_1 = 0$, while $\hat{a} = a^*, \hat{T} = T^*, \hat{T}_{reg} = T^*_{reg}, \hat{c}_2 = c^*_2, \hat{Q} = Q^*, \hat{Y}_1 = Y^*_1, \hat{Y}_2 = Y^*_2 > 0$.

The characteristic polynomial of the Jacobian at E_{4a} has root $\Lambda_1 = \sigma_B + \pi_{T|B} T^* + \frac{\pi_{D/B} D^*_m}{k_{D/B} + D^*_m} > 0$ and therefore this equilibrium (whenever it exists) is always unstable.

(b) equilibrium E_{4b} with $\hat{T} = T^* \geq 0$, while $\hat{a} = a^*, \hat{T}_{reg} = T^*_{reg}, \hat{B} = B^*, \hat{A} = A^*, \hat{c}_1 = c^*_1, \hat{c}_2 = c^*_2, \hat{Q} = Q^*, \hat{Y}_1 = Y^*_1, \hat{Y}_2 = Y^*_2 > 0$.

The characteristic polynomial of the Jacobian at E_{4b} has root $\Lambda_1 = \alpha_p + \upsilon_p\left(\frac{c^*_1}{k_D + c^*_1}\gamma_1 + \frac{c^*_2}{k_D + c^*_2}\gamma_2\right) - \frac{\nu_{D|reg}\hat{T}_{reg}}{k_{D|reg} + \hat{T}_{reg}} > \alpha_p + \upsilon_p(c^*_1\gamma_1 + c^*_2\gamma_2) - \nu_{D|reg}$. Whenever we take $\alpha_p > \nu_{D|reg}$, $\Lambda_1 > 0$ and this equilibrium (in case it exists) is unstable.

5. Finally, we consider the case $E_5 : \hat{B} = \hat{A} = \hat{c}_1 = 0$, and $\hat{D}_m = D^*_m, \hat{D}_p = D^*_p, \hat{a} = a^*, \hat{T} = T^*, \hat{T}_{reg} = T^*_{reg}, \hat{c}_2 = c^*_2, \hat{Q} = Q^*, \hat{Y}_1 = Y^*_1, \hat{Y}_2 = Y^*_2 > 0$. The characteristic polynomial of the Jacobian at E_5 has root $\Lambda_1 = \frac{\pi_{D/B} D^*_m}{D_m + k_{D/B}} + \sigma_B + \pi_{T|B} T^* > 0$ and the equilibrium (if it exists) is always unstable.

5.2. One-parameter bifurcation analysis

In Section 5.1 we have mentioned stability conclusions established analytically for a class of equilibria with a vanishing coordinate. However, due to the highly non-linear couupling of the state variables, we cannot establish analytical properties of interior equilibria of the model. Hence, we employ numerical simulations to locate and study properties of such equilibria computed by means of numerical continuation, and their possible bifurcations. The numerical analysis is based on the MATLAB toolbox MatCont [29], developed for numerical continuation of the solution branches of the system of ordinary differential equations.

In the bifurcation diagrams we employ the following convention: locally stable equilibria are marked with a solid line, unstable equilibria are marked with dashed lines. Subcritical Hopf bifurcations are marked with H^- (positive Lyapunov exponent), supercritical – with H^+ (negative Lyapunov exponent), and the periodic solution is indicated by the minima and maxima in the cycle for the respective variable. The local stability of the limit cycle is determined by the absolute value of its Floquet multipliers (an unstable limit cycle has at least one Floquet multiplier with absolute value greater than 1) [64]. We use values $\varepsilon_a = 10^{-5}, \varepsilon = 10^{-5}$ for the bifurcation diagrams in this section. The parameter values are indicated in Table 1 or in the caption of the respective bifurcation diagram.

We choose $\nu_{D|reg}$ as bifurcation parameter initially to study the effect of regulatory T cells on the activation of dendritic cells (1)-(2). At first, we use fixed values $\upsilon_m = \upsilon_p = 1$ for the bifurcation analysis of the model.

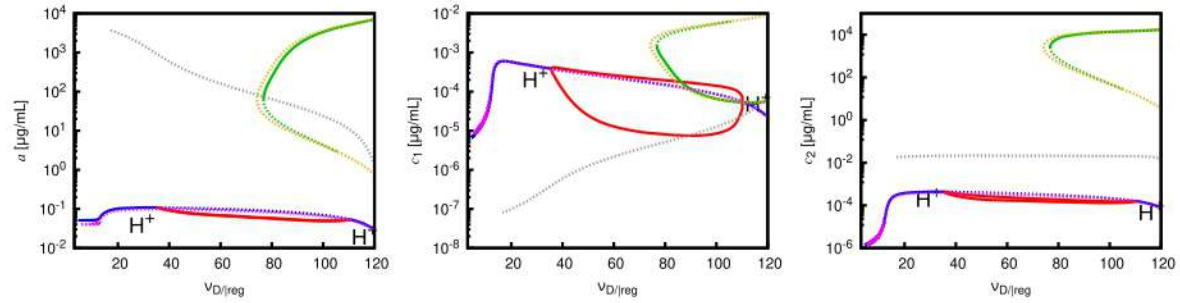

Fig. 4. Bifurcation diagram $\nu_{D|reg}$ versus apoptotic debris a, immune complexes c_1 between autoantibody and C1q, and immune complexes c_2 between C1q and apoptotic debris. The solution branch corresponding to $\hat{D}_m = 0$ is marked in grey, solution branch corresponding to $\hat{D}_p = 0$ in yellow, Hopf bifurcations occur the blue branch (red curves indicate the minima and maxima of the periodic solution). Parameters $\upsilon_m = \upsilon_p = 1$. (For interpretation of the references to colour in this figure legend, the reader is referred to the web version of this article.)

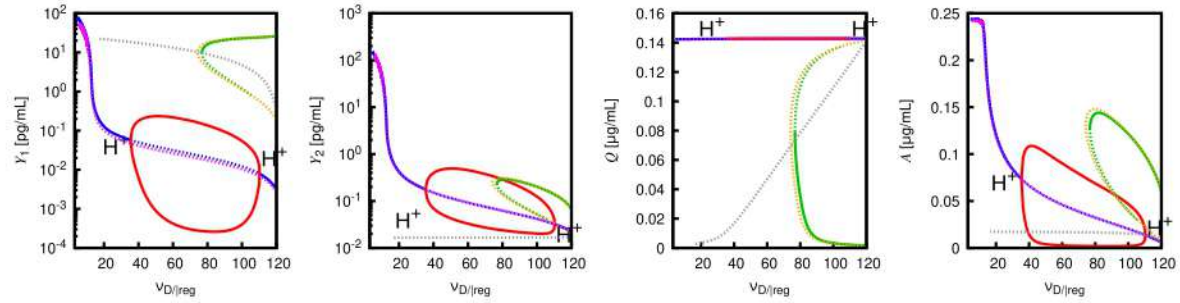

Fig. 5. Bifurcation diagram $\nu_{D|reg}$ versus pro-inflammatory cytokines Y_1, anti-inflammatory cytokines Y_2, complement protein C1q Q, autoantibody A: Hopf bifurcations occur on the blue branch (red curves indicate the minima and maxima of the periodic solution). Parameters $\upsilon_m = \upsilon_p = 1$. (For interpretation of the references to colour in this figure legend, the reader is referred to the web version of this article.)

We recall that these two parameters represent the elasticity of the mDC and pDC response to antigens and immune complexes.

There is a stable solution branch where all quantities are strictly positive, marked in blue (Fig. 4). There are two supercritical Hopf bifurcations on this branch at $\nu_{D|reg} \approx 35.335$ (Lyapunov exponent $\Lambda = -1.78 \times 10^{-5}$) and at $\nu_{D|reg} \approx 110.111$ (Lyapunov exponent $\Lambda = -3.73 \times 10^{-6}$). On the interval $\nu_{D|reg} \in (35.335, 110.111)$ there are locally asymptotically stable limit cycles (Floquet multipliers less than 1 in absolute value). We observe that for increasing values of $\nu_{D|reg}$ a region of bistability emerges for values of $\nu_{D|reg} > 76.766$. On one hand there is a locally stable limit cycle (in red), and on the other a locally stable steady state (in orange), separated by two branches of unstable equilibria (green and orange dashed). In this branch, the concentrations of apoptotic debris a and immune complexes c_2 are significantly higher than on the blue branch or on the limit cycle.

Comparing the levels of C1q Q and autoantibody A we observe a very small effect of $\nu_{D|reg}$ on the equilibria of Q on the blue branch, and on the maxima and minima of the limit cycle (red) (shown in Fig. 5). For low values $\nu_{D|reg} < 20$ on the blue branch there is a higher level of autoantibody, as expected due to the high levels of autoreactive B cells (Fig. S1 in the Supplementary material, *bottom right panel*). Nevertheless, due to the appearance of a limit cycle past the value $\nu_{D|reg} \approx 35.33$, the levels of autoreactive B cells and autoantibody increase significantly in a periodic manner, and furthermore, due to the bistability region, for values $80 < \nu_{D|reg} < 90$, the steady-state levels of autoreactive B cells and autoantibody increase significantly (steady state values on the orange branch, Fig. 5 and S1 in the Supplementary material).

The solution branches where $\hat{D}_m = 0$ (Fig. 4, grey) or $\hat{D}_p = 0$ (Fig. 4, green) are locally asymptotically unstable as we have demonstrated in Section 5.1 under some parameter relations. The numerical experiment demonstrates that these equilibria remain unstable over a larger range of $\nu_{D|reg}$.

In Fig. 6 we further investigate the bistability between two types of stable attractors: the limit cycle or the stable equilibrium by way of example for $\nu_{D|reg} = 78$. As the system is 12-dimensional, we consider the hypercube of initial values $\mathbf{Q} = \{(x_1, \ldots, x_{12}) \mid 0 \le x_i \le 10^4,\ i = 1, \ldots, 12\}$, where x_i are the model variables. We focus on this sampling domain with the aim of covering all possible initial conditions within a reasonable range. Larger or smaller hypercubes could be considered. Fig. 6 (left panel) shows the projection of $\mathbf{Q}$ onto the (a, Y_1)-plane of the two basins of attraction. We choose these phase variables in particular due to the fact that the initial values of apoptotic debris a and concentration of pro-inflammatory cytokine Y_1 are most prone to external disturbances (such as pathogenic exposure, effects of sunburn on skin, etc.), and have biological relevance for causing, for example, a SLE flare or cytokine storm. We note, however, that also the other two-dimensional or three-dimensional projections of the basins of attraction could be visualised. The right panel contains the corresponding basin stability histogram. These graphical results were obtained using the `MATLAB` toolbox `bSTAB` [30], in supervised clustering mode, using a Euclidean distance classifier. This toolbox estimates the basin stability values by Monte Carlo sampling a finite number of states, N, from a density distribution, ξ, confined to a hypercube $\mathbf{Q} \subset \mathbb{R}^D$, with $D \le 3$. The user can choose N, $\mathbf{Q}$, and ξ. In particular, we considered $N = 2000$ uniformly distributed initial conditions in $\mathbf{Q}$. We select a bounded uniform random distribution, but other options are possible, such as bounded multivariate Gaussian distribution and multivariate uniformly spaced grid sampling. Each state is numerically integrated, selecting a classical integration scheme from the MATLAB ODE suite. Refer to [65,66] for more details on the definition and computation of the basin stability values. Here we use `ode45` and we choose RelTol $= 10^{-8}$ as the relative tolerance of the numerical integration scheme. In this case, we find that the basin stability values for each attractor are $S_B(LC) \simeq 0.741$ and $S_B(FP) \simeq 0.259$, respectively, for the limit cycle and the equilibrium point. Increasing the sides of $\mathbf{Q}$, $S_B(LC)$ decreases and $S_B(FP)$ increases.

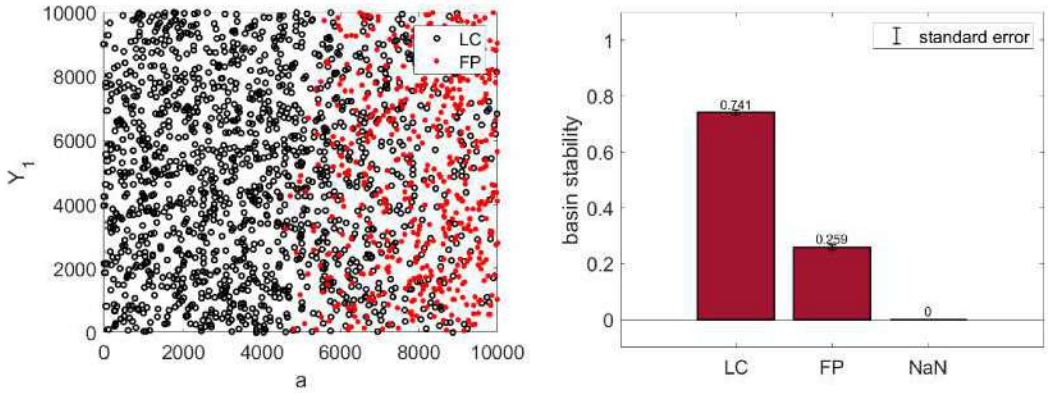

Fig. 6. Left panel: projection of basins of attraction of the limit cycle (LC) and the equilibrium point (FP) in the $a - Y_1$ plane. Right panel: basin stability histogram. The parameter values are given in Table 1, with $\nu_{D|reg} = 78$. The initial conditions are $N = 2000$ uniformly distributed points in the hypercube $\mathbf{Q} = \{(x_1, \ldots, x_{12}) \mid 0 \leq x_i \leq 10^4,\ i = 1, \ldots, 12\}$, where x_i are the twelve variables of the system. The relative tolerance of the numerical integration scheme is RelTol = 10^{-8}. Supervised clustering, with Euclidean distance classifier, is used.

Clearly, these resulting values also depend on the other selected options, such as density distribution, clustering mode, distance classifier, and numerical integrator. Our goal here is not to compare the results obtained by considering different options, but simply to visualise the basins of attraction in a particular case by way of example.

Second, we perform bifurcation analysis by varying the production rates of pro-inflammatory cytokines by mDCs and pDCs λ_0, λ_1. The bifurcation diagram for λ_0 for a fixed value of $\nu_{D|reg} = 73.017$ that is close to the region of bistability is shown in Fig. 7. There is a region of bistability for values $\lambda_0 \in (2.5, 8) \times 10^{-6}$ when $\nu_{D|reg} = 73.017$. There is a supercritical Hopf bifurcation for the value $\lambda_0 \approx 1.746 \times 10^{-6}$ (Lyapunov exponent $\Lambda = -3.12 \times 10^{-6}$), from which a branch of locally stable limit cycles is born for the range $\lambda_0 < 1.746 \times 10^{-6}$. The equilibria of the remaining model variables are shown in Fig. S2-S4 in the Supplementary material.

We present a second analysis of the basins of attraction to either stable state that are depicted in Fig. 7 by way of example for $\lambda_0 = 5$. Fig. 8 shows the projection onto the (a, Y_1)-phase plane of the basins of attraction in $\mathbf{Q}$ of the two attractors, on the left panel, and the basin stability histogram, on the right. This time, the basin stability values of the two equilibrium points are $S_B(FP_1) \simeq 0.748$ and $S_B(FP_2) \simeq 0.252$. Again, the bistability was investigated using the `bSTAB Toolbox`, in supervised clustering mode, with the same settings as described in Fig. 6.

If we take a slightly larger value for $\nu_{D|reg} = 79.143$ we see that this interval of bistability extends further to the region $0 \leq \lambda_0 < 8 \times 10^{-6}$ (Fig. S5). There, the upper branch is coloured in yellow to highlight the fact that it is in fact connected to the yellow branch shown in Fig. 4 via varying the parameter λ_0. Note that there is also an interval of λ_0 with bistability between attractors of different types: a limit cycle and an equilibrium.

The bifurcation diagram for varying λ_1 for the value $\nu_{D|reg} = 67.134$ is shown in Fig. 9. A supercritical Hopf bifurcation occurs on the blue branch at $\lambda_1 \approx 2.253 \times 10^{-5}$ (Lyapunov exponent $\Lambda = -4.95 \times 10^{-6}$). The behaviour is similar and there is a region of bistability for values $\lambda_1 \in (6 \times 10^{-5}, 10^{-4})$. Hence, the system exhibits different asymptotic behaviour over ranges of the parameters that describe the production rates of pro-inflammatory cytokines.

Next, we perform bifurcation analysis by varying the parameter ν_1 that represents the contribution of autocrine production to pro-inflammatory cytokine production. Bifurcation diagrams are shown in Fig. 10. A supercriticial Hopf bifurcation occurs at $\nu_1 \approx 10^{-5}$ (Lyapunov exponent $\Lambda = -5.73 \times 10^{-6}$). There is a narrow range of stable limit cycles for the values $\nu_1 < 10^{-5}$ on the blue branch. A narrow range of bistability between two locally stable equilibria (blue) exists for $\nu_1 \in (9 \times 10^{-5}, 1.1 \times 10^{-4})$). As far as the C1q concentration is concerned, for large values of ν_1 it is largely suppressed (Fig. 10, *left panel*). As expected, an increase in ν_1 brings an increase in the steady-state levels of pro-inflammatory cytokines Y_1 by several orders of magnitude (Fig. 10, *left panel*). The increase in the levels of anti-inflammatory cytokines Y_2 is more modest (Fig. 10, *second left panel*). There is no significant effect of the value of ν_1 on the steady-state abundance of the regulatory T cells (Fig.S10, *bottom central panel*), unless the system is in the oscillatory regime.

In Fig. 11 we show the bifurcation diagram for the parameter ν_2 that represents the inflammatory effect of the deposed in tissue immune complexes and autoantibody, after fixing the value of $\nu_{D|reg}$. For the value $\nu_{D|reg} = 67.134$, there occurs a supercritical Hopf bifurcation (Lyapunov exponent $\Lambda = 1.07 \times 10^{-5}$) at $\nu_2 \approx 2 \times 10^{-11}$. The range of values of ν_2 where a stable limit cycle occurs is $\nu_2 \in [0, 2 \times 10^{-11})$. The bistability regime range (corresponding to $\nu_2 \in (0, 1.6) \times 10^{-10}$) covers both coexistence of two stable equilibria as well as coexistence of a stable equilibrium (blue) and a stable limit cycle (red). Due to the width of the bistability range, for both small and larger values of ν_2 C1q is largely suppressed on the lower locally stable portion of the blue branch (Fig. 11, *left panel*). Similar to the previous analysis for ν_1, an increase in $\nu_2 > 1.6 \times 10^{-10}$ brings an increase in the steady-state levels of pro-inflammatory cytokines Y_1 by 2.5-orders of magnitude (Fig. 11, *second left panel*), whereas the steady-state levels of Y_2 increase by less than an order of magnitude. If we fix a smaller value $\nu_{D|reg} = 56.337$, the parameter range of ν_2 of the locally stable limit cycle becomes narrower (Fig. S12).

Again, there is no significant effect of the value of ν_2 on the steady-state abundance of the regulatory T cells (Supplementary Fig. S13 and S15, *bottom central panel*), unless the system is the oscillatory regime.

In the remainder of this section we use values $\upsilon_m = 1, \upsilon_p = 10$ for the numerical bifurcation analysis. The larger value of υ_p relative to υ_m represents a larger elasticity of the response of pDCs to antigen than mDCs. Figs. 12 and 13 represent the bifurcation diagram as $\nu_{D|reg}$ varies. The situation is similar to that represented in Fig. 4. The branch of equilibria where all quantities are strictly positive (blue) becomes unstable for values of $\nu_{D|reg} \in (35.342, 110.106)$ due to a supercritical Hopf bifurcation at $\nu_{D|reg} \approx 35.342$ (Lyapunov exponent $\Lambda = -1.3 \times 10^{-5}$), and a supercritical Hopf bifurcation at $\nu_{D|reg} \approx 110.106$ (Lyapunov exponent $\Lambda = -4.78 \times 10^{-6}$). Locally stable limit cycles exist in the vicinity of the blue branch over the interval between the two Hopf points (red curves indicate the minima and maxima of the periodic solution). Furthermore, there is a region of bistability for $\nu_{D|reg} > 91.675$ (orange branch). The range where the limit cycle exists in this case overlaps with that of the case $\upsilon_m = \upsilon_p = 1$.

As before, we perform bifurcation analysis by varying the production rates of pro-inflammatory cytokines Y_1 by mDCs and pDCs

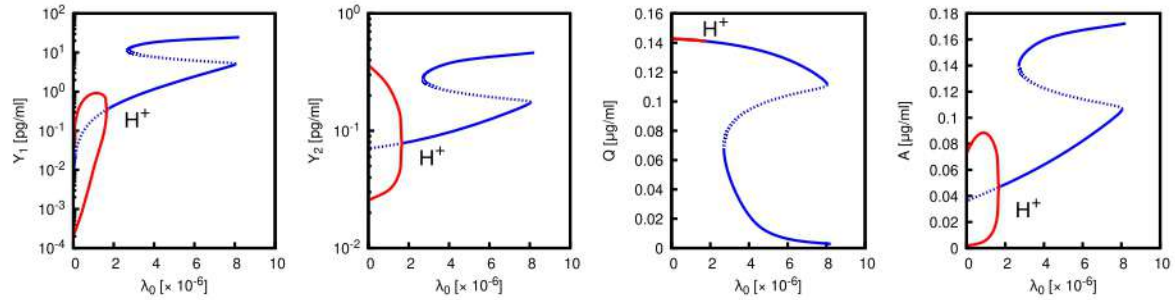

Fig. 7. Bifurcation diagram λ_0 versus pro-inflammatory cytokines Y_1, anti-inflammatory cytokines Y_2, complement protein C1q Q, autoantibody A. Fixed parameter values are $\nu_{D|reg} = 73.017, \upsilon_m = \upsilon_p = 1$: A supercritical Hopf bifurcation occurs on the blue branch (red curves indicate the minima and maxima of the periodic solution). (For interpretation of the references to colour in this figure legend, the reader is referred to the web version of this article.)

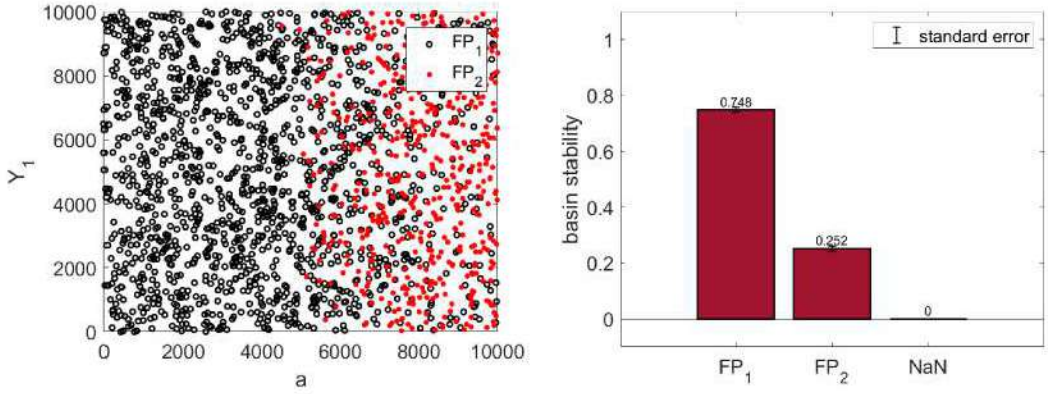

Fig. 8. Left panel: projection of basins of attraction of two equilibrium points (FP_1 and FP_2) in the $a - Y_1$ plane. Right panel: basin stability histogram. The parameter values are given in Table 1, with $\lambda_0 = 5 \times 10^{-6}$ and $\nu_{D|reg} = 73.017$. The initial conditions are $N = 2000$ uniformly distributed points in the hypercube $\mathbf{Q} = \{(x_1, \ldots, x_n) \mid 0 \le x_i \le 10^4,\ i = 1, \ldots, 12\}$, where x_i are the twelve variables of the system. The relative tolerance of the numerical integration scheme is RelTol $= 10^{-8}$. Supervised clustering, with Euclidean distance classifier, is used.

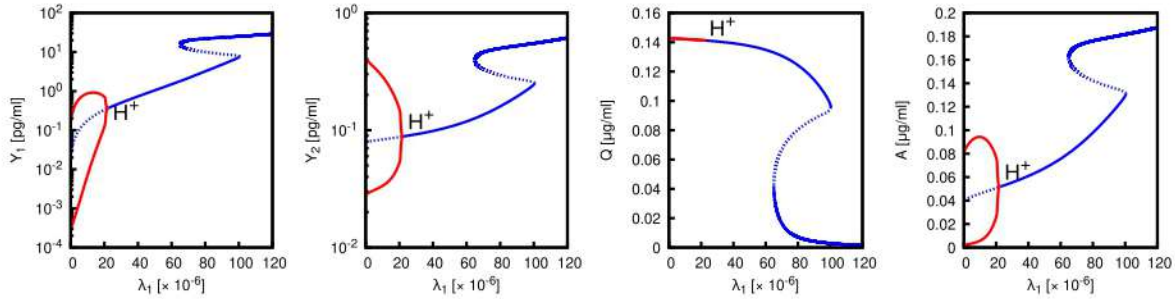

Fig. 9. Bifurcation diagram λ_1 versus pro-inflammatory cytokines Y_1, anti-inflammatory cytokines Y_2, complement protein C1q Q, autoantibody A. Fixed parameter values are $\nu_{D|reg} = 67.134, \upsilon_m = \upsilon_p = 1$: Hopf bifurcation occurs on the blue branch (red curves indicate the minima and maxima of the periodic solution). (For interpretation of the references to colour in this figure legend, the reader is referred to the web version of this article.)

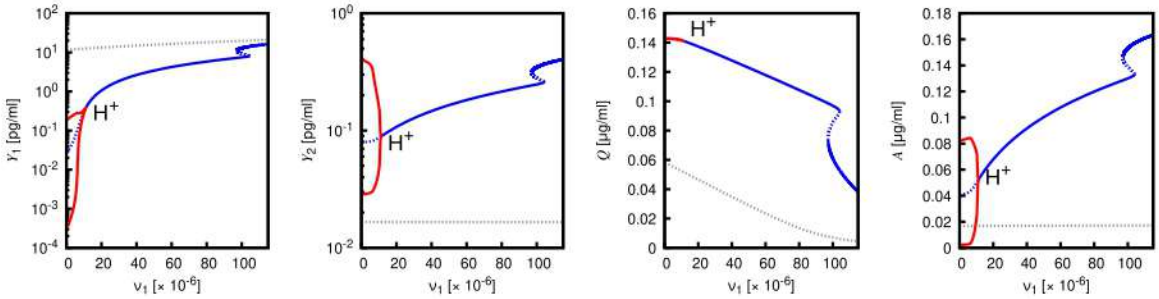

Fig. 10. Bifurcation diagram ν_1 versus pro-inflammatory cytokines Y_1, anti-inflammatory cytokines Y_2, complement protein C1q Q, autoantibody A. Fixed parameter values are $\nu_{D|reg} = 67.134, \upsilon_m = \upsilon_p = 1$. Hopf bifurcation occurs on the blue branch (red curves indicate the minima and maxima of the periodic solution). For the equilibria on the grey branch we have $\hat{D}_p = 0$. (For interpretation of the references to colour in this figure legend, the reader is referred to the web version of this article.)

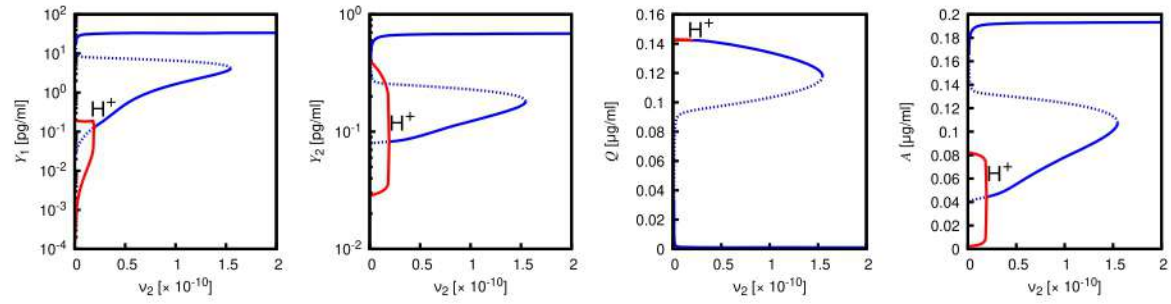

Fig. 11. Bifurcation diagram v_2 versus pro-inflammatory cytokines Y_1, anti-inflammatory cytokines Y_2, complement protein C1q Q, autoantibody A. Fixed parameter values are $v_{D|reg} = 67.134, \upsilon_m = \upsilon_p = 1$: Hopf bifurcation occurs on the blue branch (red curves indicate the minima and maxima of the periodic solution). Note that the values at equilibrium for Q stay close to 0 on the lower portion of the branch (second panel from the right). (For interpretation of the references to colour in this figure legend, the reader is referred to the web version of this article.)

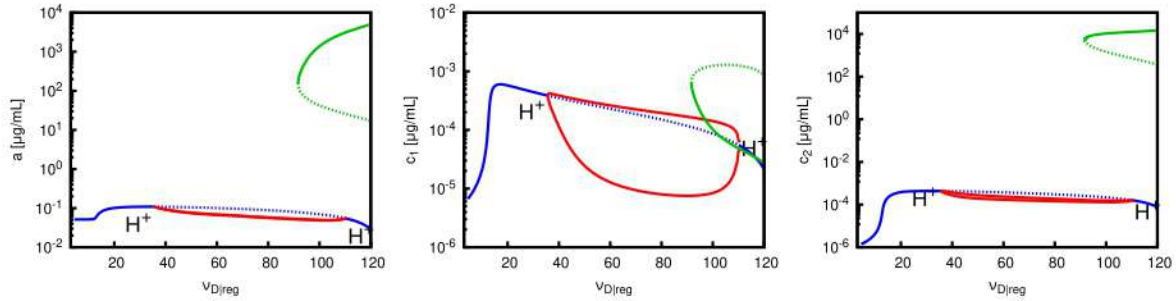

Fig. 12. Bifurcation diagram $v_{D|reg}$ versus apoptotic debris a, immune complexes c_1 between autoantibody and C1q , and immune complexes c_2 between C1q and apoptotic debris. Fixed parameters are $\upsilon_m = 1, \upsilon_p = 10$. Two supercritical Hopf bifurcations exist on the blue branch (red curves indicate the minima and maxima of the periodic solution). There is a range of bistability between different types of locally stable attractors: two fixed points (green and blue) or a fixed point (green) and a limit cycle (maxima/minima in red). (For interpretation of the references to colour in this figure legend, the reader is referred to the web version of this article.)

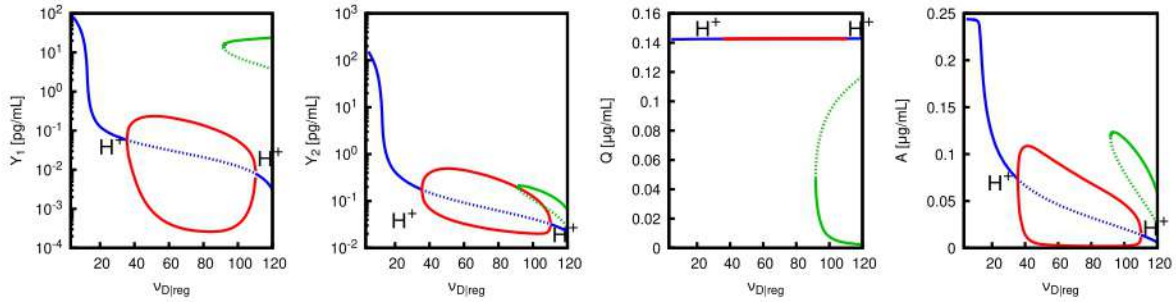

Fig. 13. Bifurcation diagram $v_{D|reg}$ versus pro-inflammatory cytokines Y_1, anti-inflammatory cytokines Y_2, complement protein C1q Q, autoantibody A. Fixed parameters are $\upsilon_m = 1, \upsilon_p = 10$. Two supercritical Hopf bifurcations on the blue branch (red curves indicate the minima and maxima of the periodic solution). There is a range of bistability between different types of locally stable attractors: two fixed points (green and blue) or a fixed point (green) and a limit cycle (maxima/minima in red). (For interpretation of the references to colour in this figure legend, the reader is referred to the web version of this article.)

λ_0, λ_1. The bifurcation diagrams for λ_0 for the values $v_{D|reg} = 85.407$ is shown in Fig. 14. There is a region of bistability for values $\lambda_0 \in (3.59 \times 10^{-6}, 1.266 \times 10^{-5})$, just beyond the point where a supercritical Hopf bifurcation occurs at $\lambda_0 \approx 1.98 \times 10^{-6}$ (Lyapunov exponent $\Lambda = -7.250641 \times 10^{-6}$). In this region of bistability there is a significant difference between the steady state levels of pro-inflammatory cytokines and autoantibody. Overall, the behaviour is similar to that of the previous case (where we considered equal activation coefficients $\upsilon_m = \upsilon_p = 1$ for the two types of dendritic cells).

The situation changes when we look into the bifurcation diagram for λ_1 (Fig. 15) with existence of multiple limit cycles. Here we start with an unstable branch of equilibria for $\lambda_1 \in (0, 9] \times 10^{-6}$ that folds onto itself at $\lambda_1 \approx 9.007$. There is a subcritical Hopf bifurcation at $\lambda_1 \approx 6.054 \times 10^{-6}$ (Lyapunov exponent $\Lambda = 2.61 \times 10^{-5}$) on the unstable equilibrium branch, at which an unstable limit cycle emerges. Unstable limit cycles (Floquet multiplier $\approx 1.37 > 1$, dotted red curve indicates the computed minima and maxima) exist in the vicinity of this branch over the range of values $\lambda_1 \in (6.054 \times 10^{-6}, 1.0556 \times 10^{-5}]$, and at $\lambda_1 = 1.0556 \times 10^{-5}$ in a fold bifurcation of limit cycles (FC) this branch of unstable limit cycles collides with a branch of stable limit cycles that exists for $\lambda_1 \in (0, 1.0556] \times 10^{-5}$ (Fig. 15, panel a).

Past the value $\lambda_1 = 5.915 \times 10^{-6}$, the blue equilibrium branch becomes locally asymptotically stable, until a supercritical Hopf bifurcation appears at $\lambda_1 \approx 1.5435 \times 10^{-5}$ (Lyapunov exponent $\Lambda = -6.22 \times 10^{-5}$). A branch of locally stable limit cycles is born at this bifurcation point $\lambda_1 \approx 1.5435 \times 10^{-5}$. There is a subcritical Hopf bifurcation on the blue branch shortly after, at $\lambda_1 \approx 1.5909 \times 10^{-5}$ (Lyapunov exponent $\Lambda = 1.12 \times 10^{-4}$). A branch of unstable limit cycles is born at $\lambda_1 \approx 1.5909 \times 10^{-5}$. The two branches collide in a fold bifurcation of limit cycles (FC) at $\lambda_1 \approx 1.5964 \times 10^{-5}$ (Fig. 15, panel b).

The blue equilibrium branch folds on itself for the third time at $\lambda_1 \approx 1.5931 \times 10^{-5}$ losing stability, while at $\lambda_1 \approx 6.578 \times 10^{-6}$ it once

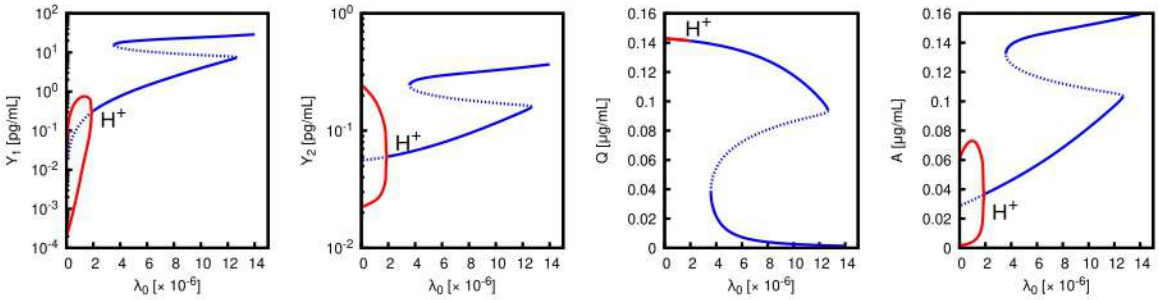

Fig. 14. Bifurcation diagram λ_0 versus pro-inflammatory cytokines Y_1, anti-inflammatory cytokines Y_2, complement protein C1q Q, autoantibody A. Fixed parameter values are $\nu_{D|reg} = 85.407, \upsilon_m = 1, \upsilon_p = 10$. Hopf bifurcations on the blue branch (red curves indicate the minima and maxima of the periodic solution). (For interpretation of the references to colour in this figure legend, the reader is referred to the web version of this article.)

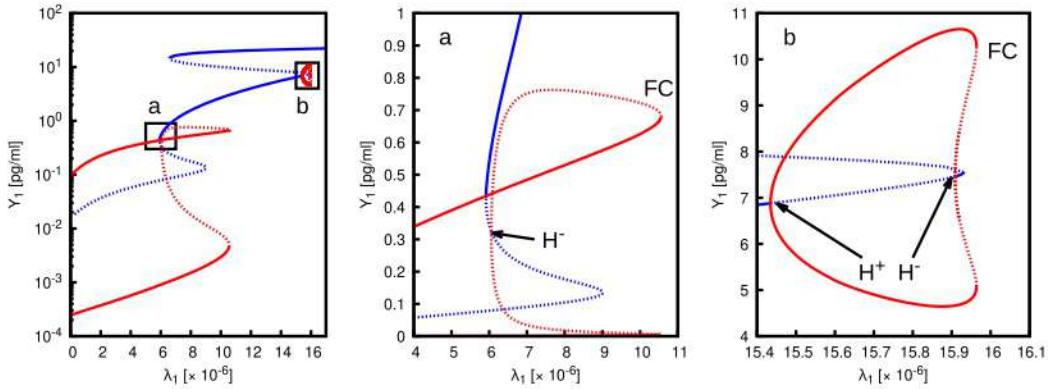

Fig. 15. Bifurcation diagram λ_1 versus pro-inflammatory cytokines Y_1 with fixed parameter values $\nu_{D|reg} = 85.407, \upsilon_m = 1, \upsilon_p = 10$. There are three Hopf bifurcations on the blue branch (two subcritical H^- and one supercritical H^+), and two fold bifurcations of limit cycles (FC). There exist two ranges of the bifurcation parameter λ_1 (enlarged view for $\lambda_1 \in [0.4, 1.1] \times 10^{-5}$ in the panel a, and for $\lambda_1 \in [1.54, 1.6] \times 10^{-5}$ in the panel b) where a pair of limit cycles – one stable (minima/maxima in solid red), one unstable (minima/maxima in dotted red) – exist in parallel. (For interpretation of the references to colour in this figure legend, the reader is referred to the web version of this article.)

again regains the local asymptotic stability. Overall, there is an interval where a tristable regime between a limit cycle and two fixed points exists (Fig. 15, leftmost panel, for the range $6.054 \times 10^{-6} < \lambda_1 < 1.0556 \times 10^{-5}$).

As done in the case $\upsilon_m = \upsilon_p = 1$, we perform bifurcation analysis by varying ν_1 for $\upsilon_m = 1, \upsilon_p = 10$ for the fixed value $\nu_{D|reg} = 85.407$ (Fig. 16). The behaviour is qualitatively similar to that noted previously. For example, on the blue branch there is a supercritical Hopf bifurcation at the value $\nu_1 \approx 8.961 \times 10^{-6}$ (Lyapunov exponent $\Lambda = -3.34 \times 10^{-6}$), leading to an interval of periodic solutions for the values $\nu_1 < 8.961 \times 10^{-6}$. Furthermore, there is a range of bistability between locally stable equilibria on the blue branches over the interval $4.1433 \times 10^{-5} < \nu_1 < 9.8167 \times 10^{-5}$.

As we choose as bifurcation parameter the rate ν_2 (Fig. 17), we see a similar situation to the one depicted in Fig. 11. A supercritical Hopf bifurcation occurs at $\nu_2 \approx 2.515 \times 10^{-11}$, and the range of the bifurcation parameter ν_2 where the limit cycle exists is $\nu_2 \in [0, 25.15] \times 10^{-12}$. However, the upper bound of the bistability regime (between two stable equilibria (blue) or between a stable equilibrium (blue) and a limit cycle (red) extends from $\nu_2 \approx 0.634 \times 10^{-12}$ to $\nu_2 \approx 1.639 \times 10^{-10}$.

Next we perform bifurcation analysis by varying the autoantibody production rate $\alpha_{B|A}$. A supercritical Hopf bifurcation (Lyapunov exponent $\Lambda = -1.34 \times 10^{-5}$) occurs on the blue branch for $\alpha_{B|A} \approx 0.015$. A branch of locally asymptotic limit cycles exists for values $\alpha_{B|A} \in [0, 0.015]$ near the lower unstable portion of the blue branch (Fig. 18). There is a range of bistability between two equilibria for the range of values $\alpha_{B|A} \in (0.015, 0.036)$ or an equilibrium and the limit cycle for the range of values $\alpha_{B|A} \in (0.004, 0.015)$.

5.3. Temporal dynamics of the model

Here we complement the bifurcation diagrams by simulations of the temporal dynamics of the model. The model is initialised with the initial values given in (18) to represent a setting where systemic inflammation in the organism is low.

Results are shown in Fig. 19 for the case $\upsilon_m = \upsilon_p = 1$. The parameter value $\nu_{D|reg} = 37$ is taken just above the value corresponding to the subcritical Hopf bifurcation H^+ on the blue curve shown in Fig. 4. For the value $\nu_{D|reg} = 37$ the system exhibits a periodic solution.

We observe that the variables converge to a steady state in an oscillatory manner for the values $\nu_{D|reg} = \{15, 25\}$ that lie before the supercritical Hopf bifurcation value. However, in Fig. 19 the values of a, c_2 at the equilibrium are monotonically increasing with respect to $\nu_{D|reg}$, as this parameter increases from 15 to 25. The maxima and minima in the limit cycle for $\nu_{D|reg} = 37$ exceed these values at equilibrium for $\nu_{D|reg} = 15$. However, as $\nu_{D|reg}$ increases further to 55 or 85, the maxima and minima (and the averaged values of a, c_2 over the cycle) decrease. Thus, the effect of $\nu_{D|reg}$ on the temporal behaviour of a, c_2 is non-monotone for the chosen set of model parameters. Analogous non-monotone behaviour for the trajectories of a, c_2 as $\nu_{D|reg}$ increases from 15 to 85 is shown in Fig. 20 for the case $\upsilon_m = 1 < \upsilon_p = 10$.

We also simulate a case where there is an sudden influx of apoptotic material by increasing $a(0)$. This influx can represent a result of ultraviolet light exposure causing keratinocyte apoptosis in the epidermis [3], resulting in a SLE flare associated with inflammation, worsening of disease symptoms which can last for weeks, and potentially causing organ damage (to the kidneys).

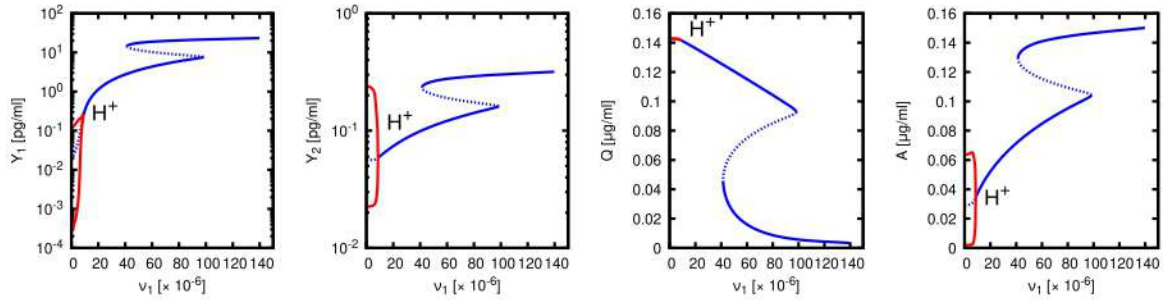

Fig. 16. Bifurcation diagram ν_1 versus pro-inflammatory cytokines Y_1, anti-inflammatory cytokines Y_2, complement protein C1q Q, autoantibody A. Fixed parameter values are $\nu_{D|reg} = 85.407, \upsilon_m = 1, \upsilon_p = 10$. There is one supercritical Hopf bifurcation on the blue branch H^+). Minima and maxima of the periodic solution are indicated in red. (For interpretation of the references to colour in this figure legend, the reader is referred to the web version of this article.)

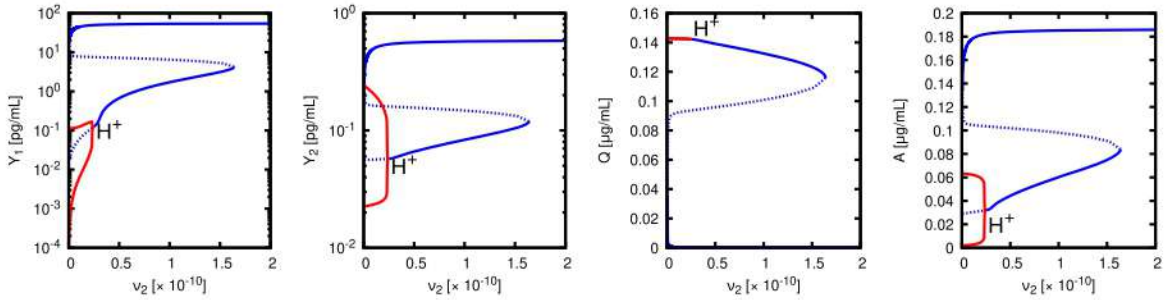

Fig. 17. Bifurcation diagram ν_2 versus pro-inflammatory cytokines Y_1, anti-inflammatory cytokines Y_2, complement protein C1q Q, autoantibody A. Fixed parameter values are $\nu_{D|reg} = 85.407, \upsilon_m = 1, \upsilon_p = 10$. There is one Hopf bifurcation on the blue branch (supercritical H^+). Minima and maxima of the periodic solution are indicated in red. (For interpretation of the references to colour in this figure legend, the reader is referred to the web version of this article.)

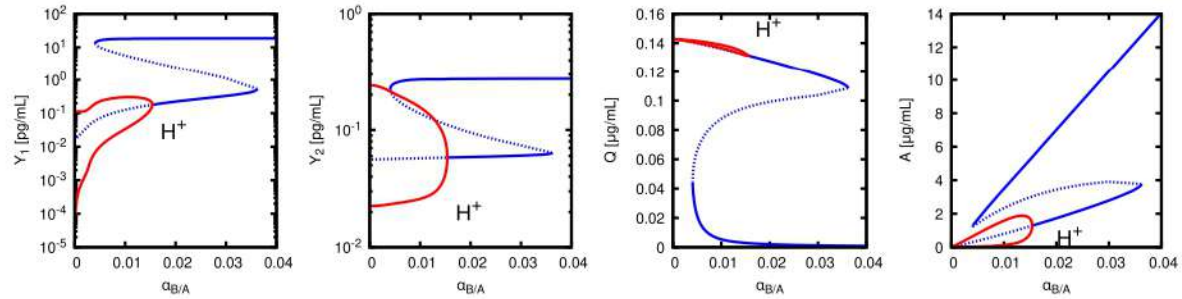

Fig. 18. Bifurcation diagram $\alpha_{B|A}$ versus pro-inflammatory cytokines Y_1, anti-inflammatory cytokines Y_2, complement protein C1q Q, autoantibody A. Fixed parameter values are $\nu_{D|reg} = 85.407, \upsilon_m = 1, \upsilon_p = 10$. There is one Hopf bifurcation on the blue branch (minima and maxima of the periodic solution are indicated in red). (For interpretation of the references to colour in this figure legend, the reader is referred to the web version of this article.)

Results of the simulation are shown in Fig. 21. The initial values for the variables except $a(0)$ are those in (18), whereas $a(0)$ varies from 10^{-5} (red), 15 (green) and 100 (blue). This introduced perturbation is able to steer the trajectory for a long time period away from the limit cycle shown in red in Fig. 21. In the limit cycle (trajectory in red) there are low values of pro-inflammatory cytokines Y_1, and immune complexes c_1, c_2. In case of the perturbation (trajectories in green, blue), there is a steady increase in the pro-inflammatory cytokines Y_1, and immune complexes c_1, c_2 that is maintained over much longer period. On the contrary, there is no significant change in the level of autoantibody A.

We study also the variation of the parameter λ_1 on the temporal dynamics of the system. We illustrate this with an initial condition the point with coordinates

$$D_m(0) = 0.045;\ D_p(0) = 0.004;\ T(0) = 1967;\ T_{reg}(0) = 1164;$$
$$B(0) = 6775;\ a(0) = 0.3224;\ A(0) = 0.004;\ Q(0) = 0.142;\ c_1(0) = 0.002,$$
$$c_2(0) = 0.003;\ Y_1(0) = 5 \times 10^{-9};\ Y_2(0) = 2.5 \times 10^{-8} \qquad (20)$$

which is located close to the fold FC of the branch with limit cycles in (Fig. 15, panel b) for $\lambda_1 \approx 1.05 \times 10^{-5}$. For the value $\lambda_1 = 1.054 \times 10^{-5}$ the solution converges to a locally stable limit cycle (Fig. 22, red). If the value of λ_1 increases beyond the value $\lambda_1 > 1.0556 \times 10^{-5}$, there are no equilibria or limit cycles beyond the local tipping point on that branch, resulting in a convergence (Fig. 22, green ($\lambda_1 = 1.5 \times 10^{-5}$) or blue ($\lambda_1 = 2 \times 10^{-5}$) curves) to the stable portion of the branch indicated in blue in Fig. 15.

The slow convergence to the steady state is due to the dominant negative eigenvalue being very small $\mathcal{O}(10^{-6})$ in absolute value (Fig. 22).

5.4. The case $D_m, D_p = 0$

As mentioned in Theorem 3, combinations of model parameters permit the asymptotic convergence of activated mDCs and pDCs D_m, D_p to zero. Here we select appropriate parameter values of $\alpha_m, \alpha_p, \upsilon_m, \upsilon_p, \nu_{D|reg}$, for which the conditions in Theorem 3 are met, and consider henceforth the case in which the role of dendritic cells in the course of the disease is not taken into account. Note that since $\alpha_m, \alpha_p, \upsilon_m, \upsilon_p, \nu_{D|reg}$ do not participate in the rest of the model equations (3)–(12), the interactions between the other components remain unchanged. The resulting system consists of ten equations and a smaller number of parameters. It is

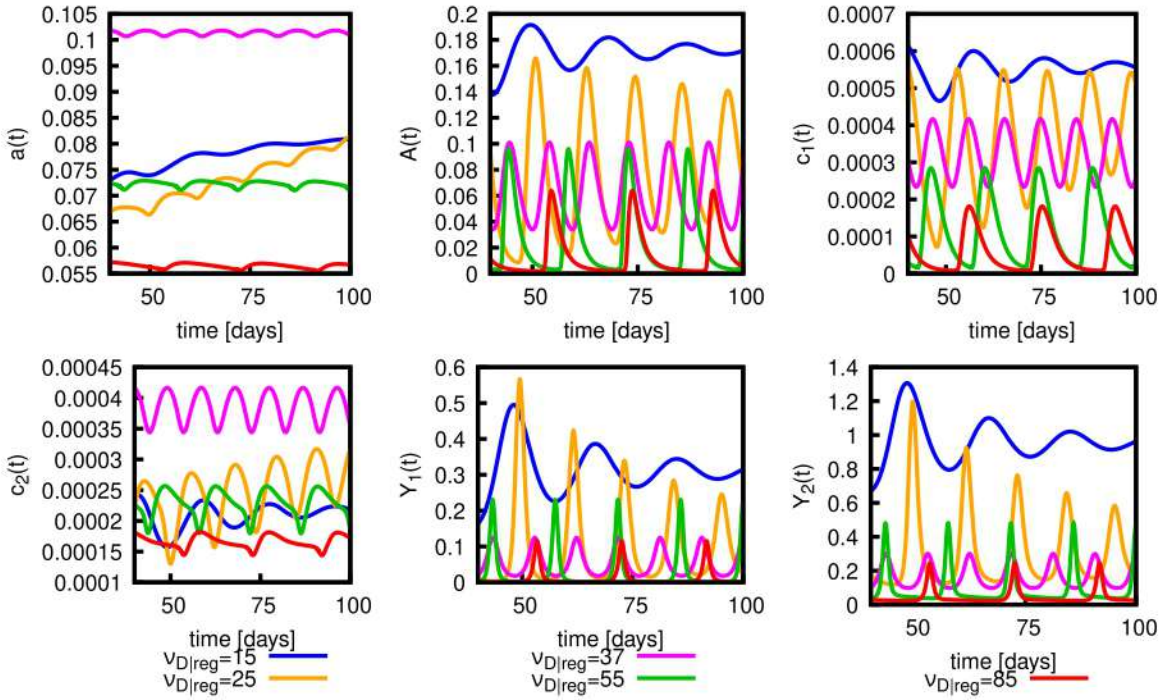

Fig. 19. Trajectories of the model for fixed parameter values $\upsilon_m = \upsilon_p = 1$ and different values of $\nu_{D|reg}$, with initial conditions (18).

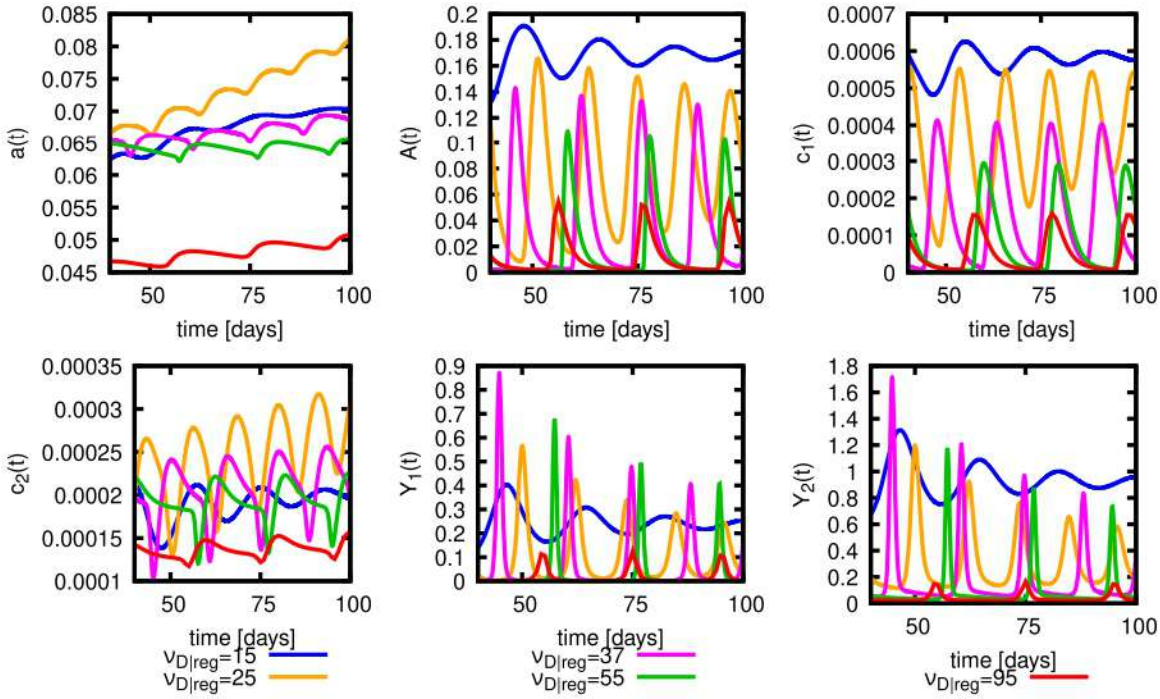

Fig. 20. Trajectories of the model for fixed parameter values $\upsilon_m = 1, \upsilon_p = 10$ and different values of $\nu_{D|reg}$, with initial conditions (18).

natural to ask whether any changes occur in the dynamics and what they are. It turns out that setting $D_m(0) = D_p(0) = 0$ from the system leads to the disappearance of one of the important properties of the model, namely periodicity in the chosen parameter regime (Table 1). This is confirmed in numerous experiments, some of which are depicted in Fig. 23.

In Fig. 23 we see that unless $\sigma_B > 0$, an autoimmune response cannot be maintained. In particular, when $\sigma_B = 0, D_m(t) = D_p(t) = 0, \forall t > 0$ autoreactive T and B cells cannot be established (Fig. S23 in Supplementary) for the parameter values listed in Table 1.

From a mathematical point of view, these results are not unexpected because the parameter that determines whether the solution is periodic or not may no longer appear in the model. Also from a biological perspective when the dendritic calls are present, $D_m, D_p > 0$, they always manage to be reactivated despite the suppressive effect of Tregs. Due to multiple factors including the high number of phase variables and non-linear coupling between them, the uncertainty in parameter values, and missing experimental observations, however, we are not in a position to demonstrate rigourously this behaviour, especially in a situation of a scracity of experimental data that can be used to

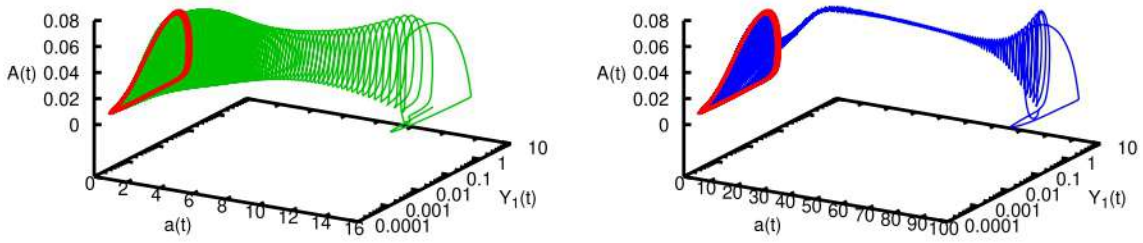

Fig. 21. Trajectories of the model projected on the (a, Y_1, A)-phase space comparing the effect of influx of apoptotic material at the initial time: $a(0) \gg 10^{-5}$ (green, blue) versus $a(0) = 10^{-5}$ (red) for fixed parameter values $\upsilon_m = 1, \upsilon_p = 10, \nu_{D|reg} = 95$. (For interpretation of the references to colour in this figure legend, the reader is referred to the web version of this article.)

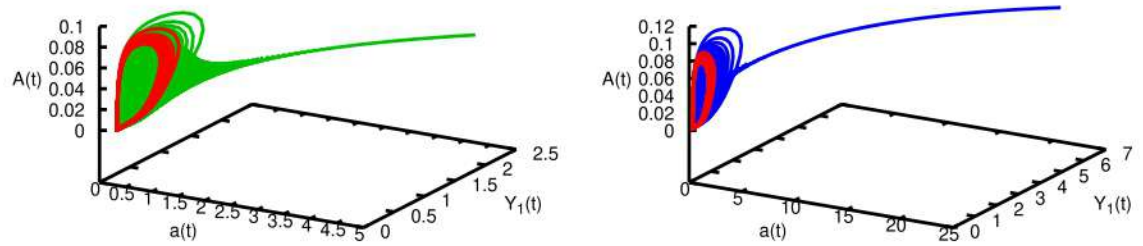

Fig. 22. Trajectories of the model projected on the (a, Y_1, A)-phase space for different values of λ_1 with initial condition (20) as follows: $\lambda_1 = 1.054 \times 10^{-5}$ (red), $\lambda_1 = 1.5 \times 10^{-5}$ (green), $\lambda_1 = 2 \times 10^{-5}$ (blue). Fixed parameters are $\nu_{D|reg} = 85.407, \upsilon_m = 1, \upsilon_p = 10$. (For interpretation of the references to colour in this figure legend, the reader is referred to the web version of this article.)

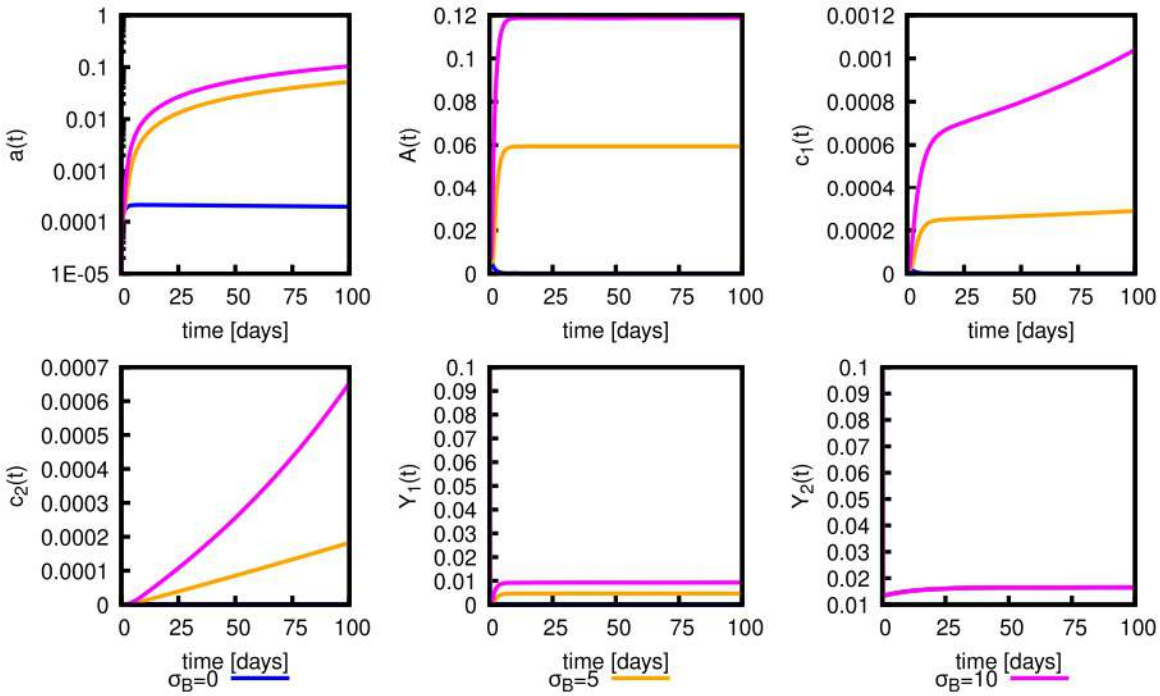

Fig. 23. Trajectories of the model comparing the cases where $D_m(t), D_p(t) \equiv 0$ for $t \geq 0$.

improve the estimated or assumed ranges and values of the model parameters.

Therefore, it is reasonable to consider the case where only pDCs do not appear in the system. It turns out that in this case the dynamics resemble that of the original model and the periodicity is maintained (as it is visible in Fig. 24). Experimental data from mice suggest that specific depletion of pDCs reduces disease manifestations such as autoantibody production [67]. Our simulation suggests the temporal dynamics of autoantibody barely changes (Fig. 24, top row), and there is a slight drop in the pro-inflammatory cytokine variable Y_1.

6. Discussion

The model for the chronic stage of SLE presented in this work is able to reproduce the persistent circulation of modified autoantigen-containing apoptotic debris that is capable of breaking self-tolerance, and is considered a hallmark of the disease [1,3]. In the model we include several components essential for the mathematical representation of the pathology chronic phase of the SLE, namely the production of autoantibody against the C1q complement protein, considered a hallmark of the disease. First, in our model we employ myeloid dendritic cells in

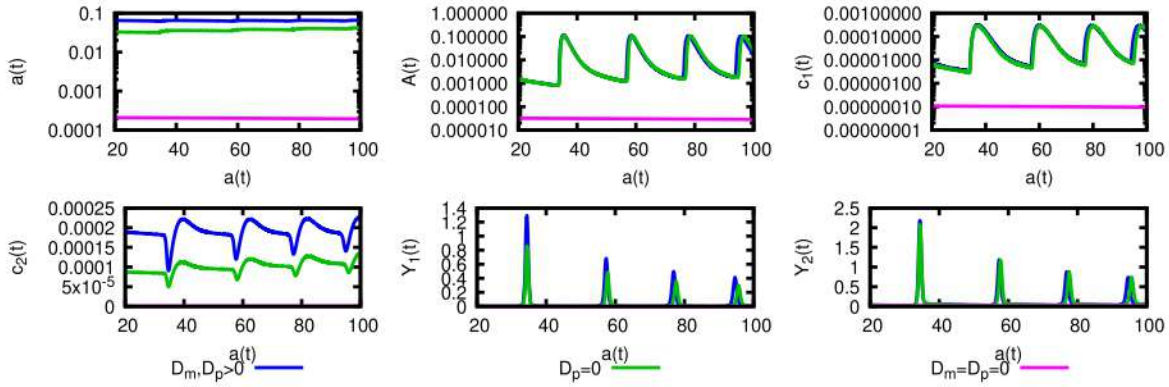

Fig. 24. Trajectories of the model comparing the cases where $D_p \equiv 0$ and $D_m, D_p > 0$ ($\nu_{D|reg} = 55, \upsilon_m = 1, \upsilon_p = 10$).

the role of antigen-presenting cells. As a result of antigen presentation, an immune response is initiated thanks to T helper cells, and regulatory T cells are responsible for its control. Autoreactive B cells activated by T helper and myeloid dendritic cells are also included in the model. Our model considers two types of antigen – with late apoptotic origin and immune complexes – both of which are able to activate dendritic cells. Furthermore, the C1q protein from the complement system forms two types of immune complexes – with the antigen with late apoptotic origin and with the autoantibody, which are represented by separate equations (9) and (10). Finally, it is important to take into consideration that the interactions described above could also be governed by molecular signals. These signals are either activating – carried out through pro-inflammatory cytokines, or deactivating – through anti-inflammatory cytokines. Our model provides a more detailed mechanistic representation of the complex processes governing the pathology of an autoimmune disease than previous models that focus on a few specific immune components [23–27].

We have demonstrated important analytic properties, namely positivity and boundedness in time of the solution of the model, that are essential for models of cellular populations. Furthermore, we have performed a local sensitivity analysis in Section 4 to explore which parameters have the highest effect on the model output. Finally, in Section 5 we have examined numerically the bifurcation structure resulting from varying parameters that display the highest sensitivity. We discuss the results mathematical findings and compare them to experimental observations on SLE in the literature to place them in a relevant immunological context.

The local sensitivity analysis of the model presented in Section 4 reveals that the model parameters with the highest sensitivity index are associated with cytokine production rates (pro- or anti-inflammatory cytokines $\lambda_{0,\dots,3}$), the C1q production rate σ_Q, and Treg activity, namely, the parameters $\nu_{D|reg}$ describing the suppressive effect of Tregs on DCs, β_2 describing the maximum conversion rate of T helper cells to Tregs due to anti-inflammatory cytokine action, and μ_{reg} describing Treg removal. Changes in these parameter values affect the most the dynamics of autoantibody A, C1q Q, apoptotic debris a and the two types of immune complexes c_1, c_2 considered in the model (Fig. 2–3). The results of our analysis can be placed in the context of defects in Tregs in autoimmune diseases that are reported in various studies. For example, the abundance of Tregs declines during the early phases of the disease [1,33], and metabolic reprogramming of Tregs in an experimental autoimmune encephalitis mouse model results in mitochondrial oxidative stress, instructing a cell death programme, causing a breakdown of self-tolerance [68]. On the other hand, treatment of SLE patients with a low-dose IL-2 has been reported to correct Treg defects and strongly expand the Treg population [69].

We have performed numerical bifurcation analysis to understand the dynamical behaviour of the model's solutions in the neighbourhood of equilibria as key parameters vary. In particular, we have focused on the effects of changes in the following parameters: the suppressive effect of Tregs on DCs $\nu_{D|reg}$, the production rates of pro-inflammatory cytokines $\lambda_0, \lambda_1, \nu_1, \nu_2$.

The bifurcation analysis shows that as $\nu_{D|reg}$ increases, the equilibrium values of apoptotic debris a and immune complex c_2 change in a non-monotone fashion, first increasing and then decreasing on the same solution branch (Fig. 4). Yet, a locally stable equilibrium eventually appears that is characterised by significantly higher concentrations of apoptotic debris a and immune complex c_2. The bifurcation analysis shows that counts of Tregs are reduced as well (Fig. S1 and Fig. S17 in the Supplementary material). We interpret this in the context of observations that pDCs exhibiting features of immune senescence and stress in SLE autoimmunity [70], and depletion of regulatory T cells [71].

As the numerical bifurcation analysis demonstrates for different model parameters (Fig. 7, 9–11, 14, 16, 17), in the regime of bistability there is a significant difference between the values of C1q concentration in equilibrium. On the other hand, when the model solution is periodic in time, the amplitude of the C1q concentration is small. The bistability property means that the dynamical system (1)–(12) can exhibit quantitatively different asymptotic behaviour in the same parameter regime depending on the system's initial value. This type of bevaviour is observed in the model for the value of C1q production rate σ_Q reported at homeostasis [56], despite the conclusion from our local sensitivity analysis that changes in Q are most sensitive to changes in σ_Q. This exploration of the dynamical behaviour suggests that for the presented model structure and the selected parameter ranges, the low levels of C1q (known as C1q deficiency observed in some SLE patients) can be understood in the context of the pathological immune interactions and outside disturbances, and need not be dependent on a reduced production of C1q in the organism. In fact, current evidence suggests that impaired clearance of apoptotic material indeed is a fundamental problem in SLE patients, and the disease is driven not by the autoantibody response but by the pathological processes that allow the exposure of autoantigen which cause immunogenicity and can be recognised by APCs, causing eventually the production of autoantibodies [45]. The pathological exposure of autoantigen has been studied mathematically by Suvandjieva et al. [20] who model processes involved in the SLE initiation stage and examine conditions leading to persistent production of autoimmunogenic material using a simple mathematical formulation.

In our model we have considered solely immune cell populations in activated state, and skipped naive and inactive states to reduce the model complexity. While some models for chronic inflammatory diseases explicitly include both naive and activated cells [72], the number of model variables and parameters becomes quite large and is not prone to analytical treatment.

We have neglected expansion of existing autoreactive B cells by letting $\sigma_B = 0$ in equation (5) because autoimmunity is assumed to arise

from the failure of checkpoints for self tolerance [73]. Although the steady-state values of both types of dendritic cells D_m, D_p appear to be low in the full model (however, the numbers of DCs in SLE patients' blood are low as well [2]), they are crucial for maintaining the existence of periodic solutions. However, in the reduced model which we have explored computationally in Section 5.4, with $D_m(0) = D_p(0) \equiv 0$, for the parameter values listed in Table 1 that concern the remaining non-zero state variables, numerical exploration reveals that the periodicity is lost and the solutions tend towards some equilibrium point. Only when we set $D_p(0) \equiv 0, \forall t > 0$ but $D_m(0) > 0$, roughly speaking in a semi-reduced model setting, the periodicity reappears for certain parameter values and the model's temporal dynamics is similar to that in the original model. This suggests that for the model structure and parameter regime considered in this work, the term $-\frac{\upsilon_{D|reg} T_{reg}}{k_{D|reg}+T_{reg}} D_m$ representing the negative feedback effect of Tregs on mDCs could be determinative for this dynamics and its absence may lead to the loss of periodicity when $D_m(0) \equiv 0$. It would be challenging, but interesting path of research to validate this observation by biological experiment.

Our model has several limitations which we discuss briefly here. First, we have not considered resting versus active states of the dendritic cells, T lymphocytes and B lymphocytes. Second, we have not considered other types of autoantibody that arise in SLE, such as anti-dsDNA antibody [45]. In addition, B cells serving as antigen-presenting cells in the autoimmunogenic context have not been considered. We have looked at a very small part of the complement system (only the recognition and initiator C1q protein) without considering possible feedback loops within the complement system involving the production of C1q by human monocyte-derived macrophages [74]. Including such additional elements could help study further interactions quantitatively, on one hand, and on the other, a wider set of data from patient's serum (cell counts and biochemistry) that can be used to finetune the parameter regime and biologically relevant phase space ranges wpuld be able to improve the model's predictive capability. Last, but not least, another possible direction for future research would be to study the effects of hormones, or to incorporate anti-inflammatory therapy or immunotherapy in the model.

CRediT authorship contribution statement

Vladimira Suvandjieva: Writing – original draft, Software, Methodology, Investigation, Formal analysis, Conceptualization; **Francesca Acotto:** Writing – original draft, Software, Investigation; **Ivanka Tsacheva:** Supervision, Conceptualization; **Peter Rashkov:** Writing – original draft, Supervision, Software, Project administration, Investigation, Funding acquisition, Conceptualization.

Funding

The work of PR and VS was supported by the Bulgarian National Science Fund [grant number KP-06-KOST/13].

Declaration of competing interest

The authors have no competing interest to declare.

Data availability

No data was used for the research described in the article.

Supplementary material

Supplementary material associated with this article can be found in the online version at 10.1016/j.mbs.2026.109832.

Appendix A.

A.1. Non-negativity of the analytic solution

Assume that the solution eventually leaves the positive orthant $\mathbb{R}^{12}_+$ and set

$$\tau := \inf_{t\geq 0}\{a(t) < 0 \vee D_m(t) < 0 \vee D_p(t) < 0 \vee T(t) < 0 \vee T_{reg}(t) < 0 \vee B(t) < 0 \vee A(t) < 0 \vee c_1(t) < 0 \vee c_2(t) < 0 \vee Q(t) < 0 \vee Y_1(t) < 0 \vee Y_2(t) < 0\}.$$

From our assumption it holds $\tau < \infty$.

Take the equation (1) for D_m. Obviously for $t \leq \tau$ we have

$$D_m'(t) \geq -\frac{\upsilon_{D|reg} T_{reg}(t)}{k_{D|reg}+T_{reg}(t)} D_m(t) - \frac{\alpha_m}{K_m} D_m^2(t) \geq -(\upsilon_{D|reg} + \frac{\alpha_m}{K_m} \max_{s\in[0,\tau]} D_m(s)) D_m(t).$$

The equation

$$\tilde{D}_m'(t) = -C_{D_m} \tilde{D}_m(t),$$

where $C_{D_m} := \upsilon_{D|reg} + \max_{s\in[0,\tau]} D_m(s)$ has the solution $\tilde{D}_m(t) \equiv 0, t \geq \tau$ if $\tilde{D}_m(\tau) = 0$. Suppose that $\tilde{D}_m(\tau) > 0$. Then there does not exist $t_0 > \tau$ such that $\tilde{D}_m(t_0) = 0$ (If there is such t_0 then $\tilde{D}_m(t) = 0, t > t_0$ which contradicts with the uniqueness of the solution.)

Having that $\tilde{D}_m(\tau) > 0$ and $\tilde{D}_m(t) \neq 0, \forall t > \tau$ the continuity of the solution implies that $\tilde{D}_m(t) > 0, \forall t > \tau$. Now, taking $\tilde{D}_m(\tau) = D_m(\tau)$ and applying the comparison theorem for ODEs we have $D_m(t) \geq \tilde{D}_m(t) > 0, \forall t > \tau$, unless $D_m(t) \equiv 0$ for all $t > 0$. The same reasoning applied to the equation (2) proves the non-negativity of D_p.

We apply similar reasoning for the equation (3) for T, noting that for $t \leq \tau$ we have

$$T'(t) \geq -\left(\frac{\beta_{reg} T_{reg}(t)}{k_{reg}+T_{reg}(t)} + \frac{\beta_2 Y_2(t)}{k_T + Y_1(t) + Y_2(t)}\right) T(t) - \beta_T T(t)^2 \geq -(\beta_{reg} + \beta_2 + \beta_T \max_{s\in[0,\tau]} T(s)) T(t)$$

we take

$$\tilde{T}'(t) = -C_T \tilde{T}(t),$$

where $C_T := \beta_{reg} + \beta_2 + \beta_T \max_{s\in[0,\tau]} T(s)$. This equation has the solution $\tilde{T}(t) \equiv 0, t > \tau$ if $\tilde{T}(\tau) = 0$. Suppose that $\tilde{T}(\tau) > 0$. Then there does not exist t_0 with the property $\tilde{T}(t_0) = 0$ because if $\tilde{T}(t_0) = 0$, then $\tilde{T}(t) = 0, t > t_0$ which contradicts with the uniqueness of the solution.

Having that $\tilde{T}(\tau) > 0$ and $\tilde{T}(t) \neq 0, \forall t > \tau$ the continuity of the solution implies that $\tilde{T}(t) > 0, \forall t > \tau$. Now, taking $T(t) \geq \tilde{T}(t) > 0$ and applying the comparison theorem for ODEs we have $T(t) \geq \tilde{T}(t) > 0, \forall t > \tau$, unless $T(t) \equiv 0$ for all $t > 0$.

For the equation (4) for T_{reg} the procedure is similar. Observing that for $t \leq \tau$,

$$T_{reg}'(t) \geq -\mu_{reg} T_{reg}(t)$$

and taking

$$\tilde{T}_{reg}'(t) = -\mu_{reg} \tilde{T}_{reg}(t).$$

we can use the previous argument to conclude positivity.

Once again we apply the same idea for the equations for B, Y_1, Y_2 with

$$\tilde{B}'(t) = -\mu_B \tilde{B}(t),$$
$$\tilde{Y}_1'(t) = -\delta_1 \tilde{Y}_1(t),$$
$$\tilde{Y}_2'(t) = -\delta_2 \tilde{Y}_2(t).$$

Now consider the equation (6) for a. For $t \leq \tau$ the following inequality holds

$$a'(t) \geq -\upsilon_{[aQ]} Q(t) a(t) - \frac{\gamma_0 a(t)}{k_D + a(t)} D_m(t) \geq -\left(\upsilon_{[aQ]} Q(t) + \frac{\gamma_0}{k_D} D_m(t)\right) a(t),$$

so there exists $\epsilon_a > 0$ such that

$$a(t) > a(\tau)\exp\left(-\int_\tau^t \left(\upsilon_{[aQ]}Q(s) + \frac{\gamma_0}{k_D}D_m(s)\right)ds\right) \geq 0, \quad t \in (\tau, \tau+\epsilon_a).$$

Now take the equation (7) for A. For $t \leq \tau$ the following inequality holds

$$A'(t) \geq -(\upsilon_{[AQ]}Q(t) + \delta_A)A(t). \tag{A.1}$$

Therefore, there exists $\epsilon_A > 0$ such that

$$A(t) > A(\tau)\exp\left(-\int_\tau^t (\upsilon_{[AQ]}Q(s) + \delta_A)ds\right) \geq 0, \quad t \in (\tau, \tau+\epsilon_A).$$

Next, we consider the equation (8) for Q. In fact,

$$Q'(t) \geq -(\upsilon_{[AQ]}A(t) + \upsilon_{[aQ]}a(t) + \delta_Q)Q(t), \quad \forall t \geq 0\,.$$

Again, there exists $\epsilon_Q > 0$ such that

$$Q(t) > Q(\tau)\exp\left(-\int_\tau^t (\upsilon_{[AQ]}A(s) + \upsilon_{[aQ]}a(s) + \delta_Q)ds\right) \geq 0, t \in (\tau, \tau+\epsilon_A).$$

For the final two equations of the system, namely for c_i, $i = 1, 2$, we have

$$c_i'(t) \geq -\left(\mu_i + \varepsilon + \gamma_i(D_m(t) + D_p(t))\right)c_i(t), \quad \forall t \leq \tau\,.$$

and hence there exist $\epsilon_i > 0$ such that

$$c_i(t) > c_i(\tau)\exp\left(-\int_\tau^t \left(\mu_i + \varepsilon + \gamma_i(D_m(s) + D_p(s))\right)ds\right) \geq 0, \quad t \in (\tau, \tau+\epsilon_i)\,.$$

These inequalities show that the solution of the system remains non-negative for $t \in [\tau, \tau+\bar{\epsilon})$ where $\bar{\epsilon} := \min\{\epsilon_a, \epsilon_A, \epsilon_Q, \epsilon_1, \epsilon_2\}$ which is a contradiction with the definition of τ. Hence, the solutions of the system stay non-negative for non-negative initial conditions.

A.2. Boundedness of the analytic solution

We start with the equation (3) for T. Clearly

$$\begin{aligned} T' \leq& \left(\frac{\pi_{T|Dm}D_m}{k_{T|Dm} + D_m} + \frac{\beta_1 Y_1}{k_T + Y_1 + Y_2}\right)T - \beta_T T^2 \leq (\pi_{T|Dm} + \beta_1)T \\ &- \beta_T T^2 = c_T T - \beta_T T^2\,, \end{aligned}$$

where we let $c_T \overset{\text{def}}{=} \pi_{T|Dm} + \beta_1$. Therefore,

$$T' \leq 2c_T T - \beta_T T^2 - c_T T \leq \frac{c_T^2}{\beta_T} - c_T T\,.$$

Gronwall's inequality implies that

$$\begin{aligned} T(t) &\leq T(0)\exp\left(\int_0^t -c_T ds\right) + \frac{c_T^2}{\beta_T}\int_0^t (e^{-c_T t + c_T s})ds \\ &= T(0)e^{-c_T t} + \frac{c_T^2}{\beta_T}\frac{1-e^{-c_T T}}{c_T} \leq \max\left\{T(0), \frac{c_T}{\beta_T}\right\} \overset{\text{def}}{=} \hat{T}, \quad \forall t \geq 0\,. \end{aligned}$$

Next we consider the equation (5) for B. Clearly

$$\begin{aligned} B' &\leq B\left(\sigma_B + \pi_{T|B}T + \pi_{Dm|B}\right) - \mu_B B^2 \\ &\leq B\left(\sigma_B + \pi_{T|B}\hat{T} + \pi_{Dm|B}\right) - \mu_B B^2 = c_B B - \mu_B B^2\,, \end{aligned}$$

where we denote $c_B \overset{\text{def}}{=} \sigma_B + \pi_{T|B}\hat{T} + \pi_{Dm|B}$. Then a similar argument 1eads to

$$B' \leq 2c_B B - \mu_B B^2 - c_B B \leq \frac{c_B^2}{\mu_B} - c_B B,$$

and Gronwall's inequality implies

$$\begin{aligned} B(t) &\leq B(0)\exp\left(\int_0^t -c_B ds\right) + \frac{c_B^2}{\mu_B}\int_0^t e^{-c_B t + c_B s}ds = \\ &= B(0)e^{-c_B t} + \frac{c_B^2}{\mu_B}\frac{1-e^{-c_B t}}{c_B} \leq \max\left\{B(0), \frac{c_B}{\mu_B}\right\} \overset{\text{def}}{=} \hat{B}, \quad \forall t \geq 0\,. \end{aligned}$$

Next, we consider the equation (8) for Q where

$$Q' \leq \sigma_Q - \delta_Q Q\,,$$

and from Gronwall's inequality we obtain that

$$\begin{aligned} Q(t) &\leq Q(0)\exp\left(\int_0^t -\delta_Q ds\right) + \sigma_Q \int_0 t e^{-\delta_Q t + \delta_Q s}ds \\ &= Q(0)e^{-\delta_Q t} + \sigma_Q\frac{1-e^{-\delta_Q t}}{\delta_Q} \leq \max\left\{B(0), \frac{\sigma_Q}{\delta_Q}\right\} \overset{\text{def}}{=} \hat{Q}, \quad \forall t \geq 0\,. \end{aligned}$$

Then we take the equation (7) for A. Note that

$$A' \leq \alpha_{B|A}\hat{B} - \delta_A A = c_A - \delta_A A\,,$$

where $c_A := \alpha_{B|A}\hat{B}$. Gronwall's inequality implies that

$$\begin{aligned} A(t) &\leq A(0)\exp\left(\int_0^t -\delta_A ds\right) + c_A\int_0^t e^{-\delta_A t + \delta_A s}ds \\ &= A(0)e^{-\delta_A t} + c_A\frac{1-e^{-\delta_A t}}{\delta_A} \leq \max\left\{A(0), \frac{c_A}{\delta_A}\right\} \overset{\text{def}}{=} \hat{A}, \quad \forall t \geq 0\,. \end{aligned}$$

Now consider the equations (8), (9) and (10). Adding all of them together gives

$$\begin{aligned} (c_1 + c_2 + Q)' \leq& \sigma_Q - (D_m + D_p)(\gamma_1 c_1 + \gamma_2 c_2) - \delta_Q Q - \frac{\mu_1 c_1 + \mu_2 c_2}{1 + \phi(c_1 + c_2)} - \varepsilon(c_1 + c_2) \\ \leq& \sigma_Q - c_{min}(c_1 + c_2 + Q)\,, \end{aligned}$$

where $c_{\min} \overset{\text{def}}{=} \min\{\varepsilon, \delta_Q\}$. Gronwall's inequality with $C(t) \overset{\text{def}}{=} c_1(t) + c_2(t) + Q(t)$ implies

$$C(t) \leq C(0)e^{-c_{min}t} + \sigma_Q\frac{1-e^{-c_{min}t}}{c_{min}} \leq \max\left\{C(0), \frac{\sigma_Q}{c_{min}}\right\}, \quad \forall t \geq 0\,.$$

Finally, considering the non-negativity of the solution (Theorem 1), we conclude that $c_1(t)$ and $c_2(t)$ are both bounded from above for all $t \geq 0$ by some positive constants $\hat{c}_1$ and $\hat{c}_2$, respectively.

From the equation (1) for D_m we obtain

$$D_m' \leq \alpha_m D_m\left(1 - \frac{D_m}{K_m}\right) + \upsilon_m(\gamma_0 + \gamma_1 + \gamma_2)D_m = \phi_m D_m - \psi_m D_m^2\,.$$

where $\phi_m \overset{\text{def}}{=} \alpha_m + \upsilon_m(\gamma_0 + \gamma_1 + \gamma_2)$ and $\psi_m \overset{\text{def}}{=} \frac{\alpha_m}{K_m}$.

Following the idea from the previous estimates on T, B, Q, we arrive to

$$D_m(t) \leq \max\left\{D_m(0), \frac{\phi_m}{\psi_m}\right\} \overset{\text{def}}{=} \hat{D}_m, \quad \forall t \geq 0\,,$$

and analogously can bound $D_p(t)$ by

$$D_p(t) \leq \max\left\{D_p(0), \frac{\phi_p}{\psi_p}\right\}, \quad \forall t \geq 0\,,$$

with $\phi_p \overset{\text{def}}{=} \alpha_p + \upsilon_p(\gamma_1 + \gamma_2)$ and $\psi_p \overset{\text{def}}{=} \frac{\alpha_p}{K_p}$.

From equation (11) we have

$$Y_1' \leq \nu_1 + \frac{\nu_2(\hat{A} + \hat{c}_1 + \hat{c}_2)}{k_1} + \lambda_0\hat{D}_m + \lambda_1\hat{D}_p - \delta_1 Y_1 = \xi_1 - \delta_1 Y_1\,,$$

where

$$\xi_1 \overset{\text{def}}{=} \nu_1 + \frac{\nu_2(\hat{A} + \hat{c}_1 + \hat{c}_2)}{k_1} + \lambda_0\hat{D}_m + \lambda_1\hat{D}_p\,.$$

As shown previously, we get

$$Y_1(t) \leq \max\left\{Y_1(0), \frac{\xi_1}{\delta_1}\right\} \overset{\text{def}}{=} \hat{Y}_1, \quad \forall t \geq 0\,.$$

Next, we consider the equation (6), for which the following estimate holds:

$$a' \leq \sigma_a\hat{Y}_1 + \sigma_A\hat{A} - \upsilon_{[aQ]}\hat{D}_m a - \varepsilon a \leq \mu_a - \varepsilon a\,,$$

with $\mu_a \overset{\text{def}}{=} \sigma_a\hat{Y}_1 + \sigma_A\hat{A}$. So,

$$a(t) \leq \max\left\{a(0), \frac{\mu_a}{\varepsilon}\right\} \overset{\text{def}}{=} a_{\max}, \quad \forall t \geq 0\,.$$

The next equation we focus on is Eq. (4). The value for $\pi_{Dm|reg}$ always can be chosen such that $\pi_{Dm|reg}\hat{D}_m < \mu_{reg}$, or

$$\pi_{Dm|reg} < \frac{\mu_{reg}\alpha_m}{K_m(\alpha_m + v_m(\gamma_0+\gamma_1+\gamma_2))}$$

and then we get:

$$T'_{reg} \le \sigma_{reg} + \beta_2\hat{T} + \pi_{Dm|reg}\hat{D}_m T_{reg} - \mu_{reg}T_{reg} = \phi_{T_{reg}} - \psi_{T_{reg}}T_{reg}\ ,$$

where $\psi_{T_{reg}} \stackrel{\text{def}}{=} \sigma_{reg} + \beta_2\hat{T}$ and $\psi_{T_{reg}} \stackrel{\text{def}}{=} \mu_{reg} - \pi_{Dm|reg}\hat{D}_m > 0$. Hence,

$$T_{reg}(t) \le \max\left\{T_{reg}(0), \frac{\phi_{T_{reg}}}{\psi_{T_{reg}}}\right\} \stackrel{\text{def}}{=} \hat{T}_{reg}, \quad \forall t \ge 0\ .$$

Finally, take the last equation (12) of the system. Here we have the following estimate:

$$Y'_2 \le \xi_{Y_2} - \delta_2 Y_2\ ,$$

where $\xi_{Y_2} \stackrel{\text{def}}{=} \lambda_2\hat{D}_m + \lambda_3\hat{T}_{reg}$ and applying Gronwall's inequality we obtain the final estimate

$$Y_2(t) \le \max\left\{Y_2(0), \frac{\xi_{Y_2}}{\delta_2}\right\} \stackrel{\text{def}}{=} \hat{Y}_2, \quad \forall t \ge 0\ . \tag{A.2}$$

References

[1] G. Tsokos, Autoimmunity and organ damage in systemic lupus erythematosus, Nat. Immunol. 21 (2020) 605–614. https://doi.org/10.1038/s41590-020-0677-6

[2] J. Fransen, J. van der Vlag, J. Ruben, G. Adema, J. Berden, L. Hilbrands, The role of dendritic cells in the pathogenesis of systemic lupus erythematosus, Arthritis Res. Ther. 12 (2010) 207. https://doi.org/10.1186/ar2966

[3] G. Tsokos, M. Lo, P. Reis, K. Sullivan, New insights into the immunopathogenesis of systemic lupus erythematosus, Nat. Rev. Rheumatol. 12 (2016) 716–730. https://doi.org/10.1038/nrrheum.2016.186

[4] M. Botto, M. Walport, C1q, autoimunity and apoptosis, Immunobiology 205 (2002) 395–406. https://doi.org/10.1078/0171-2985-00141

[5] L. Casciola-Rosen, G. Anhalt, A. Rosen, Autoantigens targeted in systemic lupus erythematosus are clustered in two populations of surface structures on apoptotic keratinocytes, J. Exp. Med. 179 (1994) 1317–1330. https://doi.org/10.1084/jem.179.4.1317

[6] C. Janeway Jr, P. Travers, M. Walport, M. Shlomchik, Immunobiology: The Immune System in Health and Disease, Garland Science, New York, 5th ed., 2001.

[7] U. Gaipl, R. Voll, A. Sheriff, S. Franz, J. Kalden, M. Herrmann, Impaired clearance of dying cells in systemic lupus erythematosus, Autoimmun. Rev. 4 (2005) 189–194. https://doi.org/10.1016/j.autrev.2004.10.007

[8] M. Botto, C. Dell'Agnola, A. Bygrave, E. Thompson, H. Cook, F. Petry, M. Loos, P. Pandolfi, M. Walport, Homozygous C1q deficiency causes glomerulonephritis associated with multiple apoptotic bodies, Nat. Genet. 19 (1998) 56–59. https://doi.org/10.1038/ng0598-56

[9] M. Schaller, C. Bigler, D. Danner, H. Ditzel, M. Trendelenburg, Autoantibodies against C1Q in systemic lupus erythematosus are antigen-driven, J. Immunol. 183 (2009) 8225–8231. https://doi.org/10.4049/jimmunol.0902642

[10] R.J.A. Goris, T.P.A. Boekhorst, J.K.S. Nuytinck, J.S.F. Gimbrère, Multiple-organ failure: generalized autodestructive inflammation?, Arch. Surg. 120 (1985) 1109–1115. https://doi.org/10.1001/archsurg.1985.01390340007001

[11] J. Dieker, L. Hilbrands, A. Thielen, H. Dijkman, J. Berden, J. van der Vlag, Enhanced activation of dendritic cells by autologous apoptotic microvesicles in MRL/LPR miceJO, Arthritis Res. Ther. 17 (2015) 103. https://doi.org/10.1186/s13075-015-0617-2

[12] H. Hirayama, K. Yoshii, H. Ojima, N. Kawai, S. Gotoh, Y. Fukuyama, Linear systems analysis of activating processes of complement system as a defense mechanism, Biosystems 39 (1996) 173–185. https://doi.org/10.1016/0303-2647(96)01617-6

[13] A. Korotaevskiy, L. Hanin, M. Khanin, Non-linear dynamics of the complement system activation, Math. Biosci. 222 (2009) 127–143. https://doi.org/10.1016/j.mbs.2009.10.003

[14] B. Liu, J. Zhang, P. Tan, D. Hsu, A. Blom, B. Leong, S. Sethi, B. Ho, J.L. Ding, P. Thiagarajan, A computational and experimental study of the regulatory mechanisms of the complement system, PLoS Comput. Biol. 7 (2011) e1001059. https://doi.org/10.1371/journal.pcbi.1001059

[15] N. Zewde, R. Gorham Jr., A. Dorado, D. Morikis, Quantitative modeling of the alternative pathway of the complement system, PLoS ONE 11 (2016) e0152337. https://doi.org/10.1371/journal.pone.0152337

[16] P. Budu-Grajdeanu, R. Schugart, A. Friedman, D. Birmingham, B. Rovin, Mathematical framework for human SLE nephritis: disease dynamics and urine biomarkers, Theor. Biol. Med. Model. 7 (2010) 14. https://doi.org/10.1186/1742-4682-7-14

[17] W. Hao, B. Rovin, A. Friedman, Mathematical model of renal interstitial fibrosis, Proc. Nat Acad. Sci. USA 111 (2014) 14193–14198. https://doi.org/10.1073/pnas.1413970111

[18] X. Gao, J. He, X. Sun, F. Li, Dynamically modeling the effective range of IL-2 dosage in the treatment of systemic lupus erythematosus, iScience 25 (2022) 104911. https://doi.org/10.1016/j.isci.2022.104911

[19] A. Yazdani, F. Bahrami, A. Pourgholaminejad, R. Moghadasali, A biological and a mathematical model of SLE treated by mesenchymal stem cells covering all the stages of the disease, Theor. Biosci. 142 (2023) 167–179. https://doi.org/10.1007/s12064-023-00390-4

[20] V. Suvandjieva, I. Tsacheva, M. Santos, G. Kararigas, P. Rashkov, Modelling the impact of NETosis during the initial stage of systemic lupus erythematosus, Bull. Math. Biol. 86 (2024) 66. https://doi.org/10.1007/s11538-024-01291-3

[21] R. Brinks, R. Fischer-Betz, S. Landwehr, M. Schneider, G. Giani, Stochastic differential equation modeling the prevalence of rare chronic diseases with an application to systemic lupus erythematosus, Stat. Neerl. 67 (2013) 202–210. https://doi.org/10.1111/stan.12003

[22] M. Mota, J. Still, J. Gamboa, E. Strobl, C. Stein, V. Kawai, T. Lasko, A data-driven approach to discover and quantify systemic lupus erythematosus etiological heterogeneity from electronic health records, AMIA Annu. Symp. Proc 2024 (2025) 172–181.

[23] R. Della Marca, M. Ramos, C. Ribiero, A. Soares, Mathematical modelling of oscillating patterns for chronic autoimmune diseases, Math. Methods Appl. Sci. 45 (2022) 7144–7161. https://doi.org/10.1002/mma.8229

[24] S. Khailaie, F. Bahrami, M. Janahmadi, P. Milanez-Almeida, J. Huehn, M. Meyer-Hermann, A mathematical model of immune activation with unified self-nonself concept, Front. Immunol. 4 (2013) 474. https://doi.org/10.3389/fimmu.2013.00474

[25] S. Khailaie, P. Robert, A. Toker, J. Huehn, M. Meyer-Hermann, A signal integration model of thymic selection and natural regulatory t cell commitment, J. Immunol. 193 (2014) 5983–5996. https://doi.org/10.4049/jimmunol.1400889

[26] M. Menale, R. Travaglini, A nonconservative kinetic model under the action of an external force field for modeling the medical treatment of autoimmune response, Commun. Nonlinear Sci. Numer. Simul. 137 (2024) 108126. https://doi.org/10.1016/j.cnsns.2024.108126

[27] M. Machado Ramos, C. Ribeiro, A. Soares, A kinetic model of t cell autoreactivity in autoimmune diseases, J. Math. Biol. 79 (2019) 2005–2031. https://doi.org/10.1007/s00285-019-01418-4

[28] K. Matsuo, Y. Iwasa, Modeling innate immunity causing chronic inflammation and tissue damage, Bull. Math. Biol. 87 (2025) 34. https://doi.org/10.1007/s11538-024-01410-0

[29] A. Dhooge, W. Govaerts, Y. Kuznetsov, H. Meijer, B. Sautois, New features of the software MatCont for bifurcation analysis of dynamical systems, Math. Comput. Modell. Dyn. Syst. 14 (2008) 147–175. https://doi.org/10.1080/13873950701742754

[30] M. Stender, N. Hoffmann, bSTAB: an open-source software for computing the basin stability of multi-stable dynamical systems, Nonlinear Dyn. 107 (2022) 1451–1468. https://doi.org/10.1007/s11071-021-06786-5

[31] K. Wendelsdorf, J. Bassaganya, R. Hontecillas, S. Eubank, Model of colonic inflammation: immune modulatory mechanisms in inflammatory bowel disease, J. Theor. Biol. 264 (2010) 1225–1239. https://doi.org/10.1016/j.jtbi.2010.03.027

[32] P. Kim, P. Lee, D. Levy, Modeling regulation mechanisms in the immune system, J. Theor. Biol. 246 (2007) 33–69. https://doi.org/10.1016/j.jtbi.2006.12.012

[33] A. Sharabi, M. Tsokos, Y. Ding, T. Malek, D. Klatzman, G. Tsokos, Regulatory T cells in the treatment of disease, Nat. Rev. Drug. Discov. 17 (2018) 823–844. https://doi.org/10.1038/nrd.2018.148

[34] K.M. Chavele, M.R. Ehrenstein, Regulatory t-cells in systemic lupus erythematosus and rheumatoid arthritis, FEBS Lett. 585 (2011) 3603–3610. https://doi.org/10.1016/j.febslet.2011.07.043

[35] K. McKenna, A. Beignon, N. Bhardwaj, Plasmacytoid dendritic cells: linking innate and adaptive immunity, J. Virol. 79 (2005) 17–27. https://doi.org/10.1128/jvi.79.1.17-27.2005

[36] S. Kim, K. Lee, B. Diamond, Follicular helper T cells in systemic lupus erythematosus, Front. Immunol. 9 (2018) 1793. https://doi.org/10.3389/fimmu.2018.01793

[37] K. Hirahara, A. Poholek, G. Vahedi, A. Laurence, Y. Kanno, J. Milner, J. O'Shea, Mechanisms underlying helper T-cell plasticity: implications for immune-mediated disease, J. Allergy Clin. Immunol. 131 (2013) 1276–1287. https://doi.org/10.1016/j.jaci.2013.03.015

[38] A. Kuhn, S. Beissert, P. Krammer, CD4$^+$ CD25$^+$ Regulatory T cells in human lupus erythematosus, Arch. Dermatol. Res. 307 (2009) 71–81. https://doi.org/10.1007/s00403-008-0891-9

[39] S. Wang, J. Wang, V. Kumar, J. Karnell, B. Naiman, P. Gross, S. Rahman, K. Zerrouki, R. Hanna, C. Morehouse, N. Holoweckyj, H. Liu, A.M.M. Team, Z. Manna, R. Goldbach-Mansky, S. Hasni, R. Siegel, M. Sanjuan, K. Streicher, M. Cancro, R. Kolbeck, R. Ettinger, IL-21 Drives expansion and plasma cell differentiation of autoreactive CD11chiT-bet+ B cells in SLE, Nat. Commun. 9 (2018) 1758. https://doi.org/10.1038/s41467-018-03750-7

[40] T. Berghe, M. Kalai, G. Denecker, A. Meeus, X. Saelens, P. Vandenabeele, Necrosis is associated with IL-6 production but apoptosis is not, Cell. Signalling 18 (2006) 328–335. https://doi.org/10.1016/j.cellsig.2005.05.003

[41] H. Anders, R. Saxena, M. Zhao, I. Parodis, J. Salmon, C. Mohan, Lupus nephritis, Nat. Rev. Dis. Primers 6 (2020) 7. https://doi.org/10.1038/s41572-019-0141-9

[42] M. Walport, K. Davies, Complement and immune complexes, Res. Immunol. 147 (1996) 103–109. https://doi.org/10.1016/0923-2494(96)87182-3

[43] M. Bijl, E. Reefman, G. Horst, P. Limburg, C. Kallenberg, Reduced uptake of apoptotic cells by macrophages in systemic lupus erythematosus correlates with decreased serum levels of complement, Ann. Rheum. Dis. 65 (2006) 57–63.

[44] U. Rabs, H. Martin, T. Hitschold, M. Golan, H. Heinz, M. Loos, Isolation and characterization of macrophage-derived C1q and its similarities to serum C1Q, Eur. J. Immunol. 16 (1986) 1183–1186.

[45] M. Trendelenburg, Autoantibodies against complement component C1Q in systemic lupus erythematosus, Clin. Transl. Immunol. 10 (2021) e1279. https://doi.org/10.1002/cti2.1279

[46] L.A. Hebert, The clearance of immune complexes from the circulation of man and other primates, Am J. Kidney Dis. 17 (1991) 352–361. https://doi.org/10.1016/S0272-6386(12)80488-4
[47] M. Baker, S. Denman-Johnson, B. Brook, I. Gaywood, M. Owen, Mathematical modelling of cytokine-mediated inflammation in rheumatoid arthritis, Math. Med. Biol. 30 (2012) 311–337. https://doi.org/10.1093/imammb/dqs026
[48] D. Santer, B. Hall, T. George, S. Tangsombatvisit, C. Liu, P. Arkwright, K. Elkon, C1q deficiency leads to the defective suppression of IFN-alpha in response to nucleoprotein containing immune complexes, J. Immunol. 185 (2010) 4738–4749. https://doi.org/10.4049/jimmunol.1001731
[49] X. Valencia, C. Yarboro, G. Illei, P. Lipsky, J Immunol. 178 (2007) 2579–2588. https://doi.org/10.4049/jimmunol.178.4.2579
[50] Merck, Human PBMC isolation and counting using the Scepter™2.0 handheld automated cell counter, 2019, (https://www.sigmaaldrich.com/deepweb/assets/sigmaaldrich/product/documents/125/255/an3311en-mk.pdf). Accessed 16.04.2025.
[51] D. Vremec, M. O'Keeffe, H. Hochrein, M. Fuchsberger, I. Caminschi, M. Lahoud, K. Shortman, Production of interferons by dendritic cells, plasmacytoid cells, natural killer cells, and interferon-producing killer dendritic cells, Immunology 109 (2006) 1165–1173. https://doi.org/10.1182/blood-2006-05-015354
[52] D. Macallan, D. Wallace, Y. Zhang, H. Ghattas, B. Asquith, C. de Lara, A. Worth, G. Panayiotakopoulos, G. Griffin, D. Tough, P.C.L. Beverley, B-cell kinetics in humans: rapid turnover of peripheral blood memory cells, Blood 105 (2005) 3633–3640. https://doi.org/10.1182/blood-2004-09-3740
[53] D. Macallan, B. Asquith, A. Irvine, D. Wallace, A. Worth, H. Ghattas, Y. Zhang, G. Griffin, D. Tough, P. Beverley, Measurement and modeling of human T cell kinetics, Eur. J. Immunol. 33 (2003) 2316–2326. https://doi.org/10.1002/eji.200323763
[54] K. Kim, G. Cho, I. Jung, Optimal treatment strategy for a tumor model under immune suppression, Comput. Math. Methods Med. 2014 (2014) 206287. https://doi.org/10.1155/2014/206287
[55] H. Lee, D. Thompson, S. Park, J. Hollenbaugh, J. Treanor, T. Mosmann, X. Jin, B. Ward, H. Miao, J. Holden-Wiltse, A. Perelson, M. Zand, H. Wu, Simulation and prediction of the adaptive immune response to influenza a virus infection, J. Virol. 83 (2009) 7151–7164. https://doi.org/10.1128/JVI.00098-09
[56] R. van Schaarenburga, J. Suurmond, K. Habets, M. Brouwer, D. Wouters, F. Kurreeman, T. Huizinga, R. Toes, L. Trouw, The production and secretion of complement component C1q by human mast cells, Mol. Immunol. 78 (2016) 164–170. https://doi.org/10.1016/j.molimm.2016.09.001
[57] R. Veerhuis, L. van Es, M. Daha, In vivo degradation of rat C1q induced by intravenous injection of soluble IgG aggregates, Immunology 54 (1985) 801–8010.
[58] T. Hibi, H. Dosch, Limiting dilution analysis of the B cell compartment in human bone marrow, Eur. J. Immunol. 16 (1986) 139–145. https://doi.org/10.1002/eji.1830160206
[59] G. Sigounas, N. Harindranath, G. Donadel, A. Notkins, Half-life of polyreactive antibodies, J. Clin. Immunol. 14 (1994) 134–140. https://doi.org/10.1007/BF01541346
[60] J. Hasskamp, J. Zapas, E. Elias, Dendritic cell counts in the peripheral blood of healthy adults, Am J. Hematol. 78 (2005) 314–315. https://doi.org/10.1002/ajh.20296
[61] M. Kaul, M. Loos, Dissection of C1q capability of interacting with IgG. time-dependent formation of a tight and only partly reversible association, J. Biol. Chem. 272 (1997) 33234–33244. https://doi.org/10.1074/jbc.272.52.33234
[62] R. Brun, P. Reichert, H. Künsch, Practical identifiability analysis of large environmental simulation models, Water Resour. Res. 37 (2001) 1015–1030. https://doi.org/10.1029/2000WR900350
[63] K. Soetaert, T. Petzoldt, Inverse modelling, sensitivity and Monte Carlo analysis in R using package FME, J. Stat. Softw. 33 (2010) 1–28. https://doi.org/10.18637/jss.v033.i03
[64] J. Guckenheimer, P. Holmes, Nonlinear Oscillations, Dynamical Systems, and Bifurcations of Vector Fields, Springer-Verlag, New York, 1983.
[65] P.J. Menck, J. Heitzig, N. Marwan, J. Kurths, How basin stability complements the linear-stability paradigm, Nat. Phys. 9 (2013) 89–92. https://doi.org/{10.1038/nphys2516}
[66] P. Menck, J. Heitzig, J. Kurths, J. Schellnhuber, How dead ends undermine power grid stability, Nat. Commun. 5 (2014) 3969. https://doi.org/10.1038/ncomms4969
[67] S. Rowland, J. Riggs, S. Gilfillan, M. Bugatti, W. Vermi, R. Kolbeck, E. Unanue, M. Sanjuan, M. Colonna, Early, transient depletion of plasmacytoid dendritic cells ameliorates autoimmunity in a lupus model, J. Exp. Med. 211 (2014) 1977–1991. https://doi.org/10.1084/jem.20132620
[68] T. Alissafi, L. Kalafati, M. Lazari, A. Filia, I. Kloukina, M. Manifava, J. Lim, V. Alexaki, N. Ktistakis, T. Doskas, G. Garinis, T. Chavakis, D. Boumpas, P. Verginis, Mitochondrial oxidative damage underlies regulatory T cell defects in autoimmunity, Cell Metab. 32 (2020) 591–604.e7. https://doi.org/10.1016/j.cmet.2020.07.001
[69] C. von Spee-Mayer, E. Siegert, D. Abdirama, A. Rose, A. Klaus, T. Alexander, P. Enghard, B. Sawitzki, F. Hiepe, A. Radbruch, G. Burmester, G. Riemekasten, J. Humrich, Low-dose interleukin-2 selectively corrects regulatory T cell defects in patients with systemic lupus erythematosus, Ann. Rheum. Dis. 75 (2016) 1407–1415. https://doi.org/10.1136/annrheumdis-2015-207776
[70] A. Psarras, A. Alase, A. Antanaviciute, I. Carr, M. Md Yusof, M. Wittmann, P. Emery, G. Tsokos, E. Vital, Functionally impaired plasmacytoid dendritic cells and non-haematopoietic sources of type I interferon characterize human autoimmunity, Nat. Commun. 11 (2020) 6149. https://doi.org/10.1038/s41467-020-19918-z
[71] M. Miyara, Z. Amoura, C. Parizot, C. Badoual, K. Dorgham, S. Trad, D. Nochy, P. Debré, J. Piette, G. Gorochov, Global natural regulatory T cell depletion in active systemic lupus erythematosus, J. Immunol. 175 (12) (2005) 8392–8400. https://doi.org/10.4049/jimmunol.175.12.8392
[72] K.V. Rogers, S.W. Martin, I. Bhattacharya, R.S.P. Singh, S. Nayak, A dynamic quantitative systems pharmacology model of inflammatory bowel disease: Part 2 – application to current therapies in Crohn's disease, Clin. Transl. Sci. 14 (2021) 249–259. https://doi.org/10.1111/cts.12850
[73] J. Suurmond, Y. Atisha-Fregoso, E. Marasco, A.N. Barlev, N. Ahmed, S.A. Calderon, M.Y. Wong, M.C. Mackay, C. Aranow, B. Diamond, Loss of an IgG plasma cell checkpoint in patients with lupus, J. Allergy Clin. Immunol. 143 (5) (2019) 1586–1597. https://doi.org/10.1016/j.jaci.2018.10.041
[74] S. Thanei, M. Trendelenburg, Anti-C1Q autoantibodies from patients with systemic lupus erythematosus induce C1Q production by macrophages, J. Leukoc. Biol. 101 (2017) 481–491. https://doi.org/10.1189/jlb.3A1215-535R